

Accepted Manuscript

Cretaceous-Cenozoic growth of the Patagonian broken foreland basin, Argentina: Chronostratigraphic framework and provenance variations during transitions in Andean subduction dynamics

Kristina L. Butler, Brian K. Horton, Andrés Echaurren, Andrés Folguera, Facundo Fuentes

PII: S0895-9811(19)30017-3

DOI: <https://doi.org/10.1016/j.jsames.2019.102242>

Article Number: 102242

Reference: SAMES 102242

To appear in: *Journal of South American Earth Sciences*

Received Date: 9 January 2019

Revised Date: 6 June 2019

Accepted Date: 21 June 2019

Please cite this article as: Butler, K.L., Horton, B.K., Echaurren, André., Folguera, André., Fuentes, F., Cretaceous-Cenozoic growth of the Patagonian broken foreland basin, Argentina: Chronostratigraphic framework and provenance variations during transitions in Andean subduction dynamics, *Journal of South American Earth Sciences* (2019), doi: <https://doi.org/10.1016/j.jsames.2019.102242>.

This is a PDF file of an unedited manuscript that has been accepted for publication. As a service to our customers we are providing this early version of the manuscript. The manuscript will undergo copyediting, typesetting, and review of the resulting proof before it is published in its final form. Please note that during the production process errors may be discovered which could affect the content, and all legal disclaimers that apply to the journal pertain.



1 **Cretaceous-Cenozoic growth of the Patagonian broken foreland basin, Argentina:**
2 **Chronostratigraphic framework and provenance variations during transitions in Andean**
3 **subduction dynamics**

4

5 Kristina L. Butler*^{1,2}, Brian K. Horton^{1,2}, Andrés Echaurren³, Andrés Folguera³, Facundo
6 Fuentes⁴

7

8 ¹Department of Geological Sciences, Jackson School of Geosciences, University of Texas at
9 Austin, Austin, TX, USA

10 ²Institute for Geophysics, Jackson School of Geosciences, University of Texas at Austin, Austin,
11 TX, USA

12 ³Instituto de Estudios Andinos, Facultad de Ciencias Exactas y Naturales, Universidad de
13 Buenos Aires-CONICET, Buenos Aires, Argentina

14 ⁴YPF S.A., 515 Macacha Güemes, Buenos Aires, Argentina

15

16 *Corresponding author.

17 E-mail address: kristina.butler@utexas.edu

18

19 Keywords: Andes; Patagonia; foreland basin; provenance; U-Pb geochronology; Hf isotopes

20

21 *Journal of South American Earth Sciences* Special Issue: *Tectonics of Patagonian Basins*.

22 Original version submitted: January 9, 2019

23 Revised version submitted: June 5, 2019

24

25 **Key Points: 3–5 points, <85 characters each**

26 (1) Detrital zircon U-Pb ages demonstrate Late Cretaceous reversal in sediment polarity

27 (2) Depositional ages for growth strata constrain thrust-belt and intraforeland uplift

28 (3) Hf isotopes record tectonic reorganization and overriding plate deformational mode

29 **Abstract**

30

31 The Cretaceous-Cenozoic evolution of the Patagonian broken foreland basin system at
32 42-43°S in the northern Chubut province of Argentina is associated with variable retroarc phases
33 of fold-thrust belt shortening, extension, and basement uplift during changes in the dynamics of
34 oceanic slab subduction. Basement inheritance and progressive shallowing of an east-dipping
35 subducting slab are important mechanisms of foreland partitioning, as dictated by the preexisting
36 (pre-Andean) structural architecture and forelandward (eastward) advance of Late Cretaceous arc
37 magmatism. Previously recognized growth strata help define the timing of fold-thrust belt
38 shortening and retroarc basement-involved uplift, but the precise consequences for sediment
39 routing remain poorly understood, with uncertainties in patterns of basin evolution before,
40 during, and after shallowing and resteepeening of the subducting slab.

41 In this study, distinctive sediment source regions and magmatic histories enable
42 evaluation of the stratigraphic and tectonic evolution of the retroarc foreland basin using new
43 provenance results, maximum depositional ages, and isotopic signatures from detrital zircon U-
44 Pb geochronology and Lu-Hf geochemical analyses. A compilation of published bedrock
45 crystallization ages and distributions of metamorphic and igneous basement rocks identify: a
46 western source region defined by the Andean magmatic arc and associated pre-Andean
47 basement; and an eastern source region consisting of intraplate magmatic units and the North
48 Patagonian Massif.

49 We demonstrate that Aptian-Cenomanian retroarc basin fill was derived principally from
50 the basement massif and intraplate volcanic units to the east, followed by a Late Cretaceous
51 (Campanian-Maastrichtian) reversal in sedimentary polarity and subsequent exclusive derivation

52 from the Andean arc and orogenic belt to the west. Late Cretaceous-Paleocene slab shallowing
53 and arc cessation was succeeded by late Eocene–earliest Miocene extension during slab rollback
54 and renewal of arc magmatism. Thereafter, Miocene sedimentation was closely linked to
55 shortening in the Andean fold-thrust belt. Within the retroarc succession, new U-Pb ages
56 provide estimates of depositional ages for Lower Cretaceous through Miocene stratigraphic
57 units.

58 Finally, in addition to U-Pb provenance and chronostratigraphic constraints, zircon Hf
59 isotopic signatures from the detrital record provide confirmation of a Cretaceous-Cenozoic
60 history involving: (1) initial establishment of a continental magmatic arc; (2) transition from a
61 neutral to compressive tectonic regime; (3) shallowing of the subducting slab and arc cessation
62 during retroarc basement partitioning; (4) arc retreat and foreland basin abandonment during slab
63 rollback (with modest extension and crustal thinning); and (5) final renewed shortening during
64 arc rejuvenation.

65

66 **1. Introduction**

67

68 The Andean retroarc foreland of northern Patagonia (Fig. 1) records a complex
69 Mesozoic-Cenozoic history of subduction-related contractional, extensional, and neutral tectonic
70 regimes during variable phases of basin genesis, arc magmatism, and convergent-margin
71 geodynamics. The Patagonian broken foreland is situated between two well-studied Andean
72 foreland basins, the Neuquén basin to the north and the Magallanes-Austral basin to the south
73 (Horton, 2018a and references therein), and is bordered by large basement provinces defined by
74 the Deseado and North Patagonians massifs. The basement massifs and adjacent broken foreland

75 region (Fig. 1) preserve important records of deformation, magmatism, and sedimentation before
76 and during Andean orogenesis (Franzese et al., 2003; Pankhurst et al., 2006; Ramos, 2008).
77 Inherited structures accommodated Andean shortening in both hinterland and retroarc regions
78 through the reactivation of basement-involved faults and inversion of former extensional basins
79 (Giacosa and Heredia, 2004; Echaurren et al., 2016). Contrasting phases of shortening and
80 extension are likely linked to differences in coupling of the downgoing and overriding plates
81 during shallowing and resteeptening of the subducting slab (Horton and Fuentes, 2016; Horton,
82 2018b), as expressed in the irregular Late Cretaceous inboard advance, Paleocene-middle Eocene
83 cessation, and middle-Eocene–Miocene trenchward retreat and broadening of arc magmatism
84 (Folguera and Ramos, 2011; Gianni et al., 2018). Episodes of Paleocene-Eocene intraplate
85 volcanism may be related to slab window genesis or lithospheric removal (Muñoz et al., 2000; de
86 Ignacio et al., 2001; Aragón et al., 2011b; 2013; Kay et al., 2007; Zaffarana et al., 2012; Iannelli
87 et al., 2018).

88 The Andean history of the North Patagonian region involved the development of a fold-
89 thrust belt (Giacosa and Heredia, 2004; Giacosa et al., 2005; García Morabito and Ramos, 2012),
90 structural partitioning of the adjacent foreland basin (Bilmes et al., 2013; Gianni et al., 2015;
91 Echaurren et al., 2016; Savignano et al., 2016; Franzese et al., 2018), and evolution of the
92 magmatic arc linked to variations in slab dip (Pankhurst et al., 1999; Suárez and de la Cruz,
93 2001; Folguera and Ramos, 2011; Echaurren et al., 2016, 2017; Gianni et al., 2018; Folguera et
94 al., 2018a, 2018b; Fernández Paz et al., 2018). However, most of the prevailing tectonic models
95 have been proposed on the basis of structural and magmatic records, with limited information
96 regarding sedimentary basin dynamics (i.e., timing of deposition, duration of stratigraphic
97 hiatuses, and potential shifts in sedimentary provenance). Such information would shed light on

98 basin generation mechanisms in the context of the previously proposed tectonic framework for
99 this segment of the Andean margin, with implications for alternating tectonic regimes
100 (shortening, extension, and stasis), continental crustal budgets (crustal thickening and thinning),
101 subduction dynamics (slab shallowing and resteepeening), and magmatic arc behavior (advance,
102 retreat, cessation, and rejuvenation).

103 Here we integrate regional stratigraphic and geologic constraints with new detrital zircon
104 U-Pb geochronological results for 14 samples from Cretaceous-Cenozoic retroarc successions
105 that span proposed phases of slab shallowing and resteepeening in the northern segment (42-43°S)
106 of the Patagonian broken foreland basin (Fig. 2). These data provide insights into provenance
107 variations during shifts in deformational mode within the overriding plate, as well as new
108 chronostratigraphic constraints for Cretaceous through Neogene basin fill (Fig. 3). We also
109 evaluate the Lu-Hf isotope geochemistry of 4 detrital zircon samples to investigate crustal
110 evolution trends over a broad period (~200–10 Ma) encompassing several transitions in
111 subduction dynamics. Our results point to a first-order control of Andean orogenesis and
112 subduction processes on sediment source regions, including a change from an eastern basement
113 source to a western Andean source during proposed Late Cretaceous slab shallowing. Moreover,
114 crustal evolution trends in the North Patagonian retroarc region reflect fluctuating tectonic
115 regimes that define contrasting stages of basin evolution linked to variable extension and
116 shortening.

117

118 **2. Geologic setting**

119

120 *2.1. Modern configuration*

121
122 The Andean orogenic profile across northern Patagonia (Fig. 1) includes a western
123 forearc region (Coastal Cordillera and Central Valley), Andean magmatic arc (North Patagonian
124 Andes), a relatively low elevation (<2 km) fold-thrust belt (Patagonian Precordillera), and a wide
125 (~400 km) foreland partitioned by basement-involved structures (Patagonian broken foreland
126 basin) in the east. The North Patagonian Andes are situated north of the Nazca-Antarctic-South
127 American triple junction at ~46.5°S, where the Chile Rise spreading center intersects the trench.
128 The Liquiñe-Ofqui fault zone (LOFZ) is a continuous (~1000 km long) intra-arc right-lateral
129 strike-slip fault that accommodated oblique convergence and enhanced Neogene-Quaternary
130 magmatism and denudation (Hervé, 1994; Thomson, 2002; Andriasola et al., 2005). The
131 Patagonian broken foreland basin is flanked by two basement provinces, the North Patagonian
132 (or Somún Cura) massif and the Deseado massif, and is situated between two well-studied
133 Andean retroarc foreland basins, the Neuquén basin to the north and the Magallanes-Austral
134 basin to the south (e.g., Biddle et al, 1986; Howell et al, 2005; Romans et al., 2011; Fosdick et
135 al., 2011; Ghiglione et al., 2010; Balgord and Carrapa, 2016; Horton et al., 2016; Schwartz et al.,
136 2017).

137

138 *2.2. Retroarc foreland basin*

139

140 The Patagonian broken foreland (Fig. 2) hosts a Lower Cretaceous through Miocene
141 clastic succession punctuated by two depositional hiatuses and extensive igneous units (Fig. 3).
142 The nonmarine Lower Cretaceous Chubut Group comprises principally fluvial deposits with
143 local volcanoclastic facies and is divided into the Los Adobes and Cerro Barcino Formations

144 (Marveggio and Llorens, 2013; Figari et al, 2015; Suárez et al., 2014; Navarro et al., 2015). A
145 depositional hiatus separates the Chubut Group from the overlying marginal marine Upper
146 Cretaceous-lower Paleogene Paso del Sapo and Lefipán Formations (Spalletti, 1996; Scasso et
147 al., 2012). Locally, the Paso del Sapo Formation directly overlies igneous rocks of the Jurassic
148 Lonco Trapial Formation. An additional depositional hiatus, of late Paleocene–Oligocene age, is
149 coeval with volcanic emplacement of the Pilcaniyeu Belt (Huitrera Formation) and El Maitén
150 Belt (Ventana Formation) (Rapela et al., 1988; Aragón et al., 2011b; 2013). The youngest basin
151 fill of the Patagonian broken foreland (Fig. 3) unconformably overlies the Paso del Sapo-Lefipán
152 sedimentary succession and Huitrera-Ventana volcanic deposits, and is composed of Miocene
153 fluvial, lacustrine, and alluvial-fan deposits of the Ñirihuau, La Pava, and Collón Curá
154 Formations (Bilmes et al, 2014; Bechis et al., 2014; Echaurren et al., 2016; Bucher et al, 2018).

155

156 *2.3. Foreland basement*

157

158 Crystalline basement of northern Patagonia (Figs. 1 and 2) consists of Paleozoic-
159 Mesozoic metamorphic complexes and igneous suites (Fig. 4). Metamorphic basement is
160 exposed on the eastern flank of the North Patagonian Andes within the fold-thrust belt (~41-
161 42°S, Colohuincul Complex; Hervé et al., 2018). In the retroarc zone, the North Patagonian
162 Massif defines a broad and discontinuous region (~71-66°W) of Paleozoic-Triassic metamorphic
163 and igneous basement units (Fig. 2 and 4). This massif is capped by a voluminous Jurassic
164 rhyolitic ignimbrite (V1 volcanic stage deposits of the Marifil Formation; Pankhurst et al., 2000,
165 2006). Prior to the main phase of Andean shortening, prolonged Late Triassic–Early Cretaceous
166 extension was associated with Gondwana breakup and opening of the South Atlantic (Franzese et

167 al., 2003; Ramos, 2009). Mesozoic normal faults bounding extensional basins (e.g., the Early
168 Jurassic Cañadón Asfalto Basin; Hauser et al., 2017) were later reactivated during Andean
169 shortening in hinterland and foreland regions (Bilmes et al., 2013; Echaurren et al., 2016).

170

171 *2.4. Fold-thrust belt*

172

173 The North Patagonian fold-thrust belt (Figs. 1 and 2) is a narrow (<100 km), low-
174 elevation (<2 km) basement-involved zone of dominantly east-directed thrust faults and
175 subordinate west-directed backthrusts (Giacosa and Heredia, 2004). The decollement is rooted
176 in pre-Mesozoic basement at ~15 km depth (Colohuincul Complex; Echaurren et al., 2016).
177 Total shortening did not exceed ~20 km (<16%, Orts et al., 2015). Thrust sheets involve
178 Jurassic-Cretaceous arc-related plutonic rocks (North Patagonian Batholith and the
179 Subcordilleran Belt), Jurassic sedimentary and volcanic units (Pilquitrón Formation), and
180 Cenozoic volcanic rocks of the Paleocene-Eocene Pilcaniyeu Belt (Huitrera Formation) and
181 Eocene-lowermost Miocene El Maitén Belt (Ventana Formation). The hinterland recorded two
182 phases of shortening (Cretaceous-Paleocene and Miocene) and an intervening period of
183 extension (Oligocene-earliest Miocene). The earliest episode of shortening is recognized as
184 Aptian-Albian, as defined by an angular unconformity between Lower Jurassic units and the
185 overlying Cretaceous Divisadero Group (Suaréz et al., 2009, 2010; Echaurren et al., 2016, 2017).
186 Oligocene-early Miocene extension across forearc and retroarc regions at 40-42°S is recognized
187 by a strong positive gravity anomaly and seismically imaged low-angle normal faults (Spalletti
188 and Dalla Salda, 1996; Muñoz et al, 1998; Jordan et al, 2001). The main phase of shortening and
189 fold-thrust belt development is constrained to the middle-late Miocene by apatite fission-track

190 cooling ages and growth strata involving the Collón Curá and Ñirihuau Formations (Fig. 3;
191 Thomson et al., 2001; Giacosa and Heredia, 2004; Ramos et al, 2015).

192

193 *2.5. Magmatic arc*

194

195 In northern Patagonia, the Andean magmatic arc (Figs. 1 and 2) is composed of the calc-
196 alkaline North Patagonian Batholith (41-46°30'S) and its volcanic equivalents (Fig. 4). Granitic
197 suites intruded progressively shallower crustal levels from Late Jurassic to late Miocene time,
198 with a main phase of mid-Cretaceous emplacement broadly coincident with early Andean
199 shortening (~135-80 Ma, Pankhurst et al., 1999; Suárez and de la Cruz, 2001; Andriasola et al.,
200 2005; Aragón et al., 2011a; Castro et al., 2011).

201

202 **3. Sediment source regions**

203

204 A compilation of published isotopic ages and detrital zircon age distributions for
205 crystalline bedrock and metamorphic units (Fig. 4) characterizes sediment source regions for the
206 Cretaceous–Neogene Patagonian broken foreland, including western sources (North Patagonian
207 Andes) and eastern sources (North Patagonian Massif and Mesozoic-Cenozoic intraplate
208 volcanic units).

209

210 *3.1. Basement*

211

212 Basement rocks crop out in the both the western hinterland (including a Paleozoic
213 accretionary complex, Colohuincul Complex, and Devonian intrusive rocks) and eastern retroarc
214 region (the North Patagonian Massif consisting of Paleozoic metamorphic rocks and plutonic
215 suites). These basement units yield a broad range of overlapping Paleozoic ages, with common
216 age peaks centered around 530-520, 475-465, 400-390, 375-365, 330-320, 290-280, and 260-250
217 Ma (Fig. 4B).

218

219 *3.2. Magmatic arc units*

220

221 Mesozoic-Cenozoic subduction along the western margin of South America produced
222 magmatic arc plutonic suites and volcanic equivalents (Figs. 2 and 4). The oldest of these is the
223 Late Triassic Central Patagonian Batholith (~222-206 Ma), a NW-trending granitic belt exposed
224 within the modern foreland (Rapela et al, 1992; Zaffarana et al, 2014). The Early Jurassic
225 Subcordilleran Belt (~185-181 Ma) is a NNW-trending granitic belt exposed within the Andean
226 fold-thrust belt (Rapela et al, 2005). The granitic North Patagonian Batholith (~173-5 Ma)
227 recorded much of the Cretaceous-Cenozoic activity of the Andean magmatic arc (González Díaz,
228 1982; Pankhurst et al, 1984; Pankhurst et al, 1999; Rolando et al, 2002; Rolando et al, 2004;
229 Aragón et al, 2011a; Castro et al, 2011). Volcanic equivalents of the North Patagonian Batholith
230 include: dacitic-rhyolitic ignimbrites and associated pyroclastic products of the Lago la Plata
231 Formation (~153-136; Suárez et al., 2009a); the andesitic-dacitic-rhyolitic Divisadero Group
232 (~118-105 Ma; Suárez et al., 2009b and 2010; Aragón et al., 2011a; Echaurren et al., 2017),
233 andesitic-dacitic Don Juan Formation (~91 Ma; Franchi and Page, 1980); recently identified
234 calc-alkaline dacites near Gastre (~76-74 Ma; Zaffarana et al., 2018); and the subalkaline to

235 tholeiitic El Maitén Belt (~37-20 Ma; Fernández Paz, 2018; Rapela et al., 1988; Bechis et al.,
236 2014). The Lago la Plata Formation, Divisadero Group and El Maitén Belt are exposed today
237 along the eastern slope of the North Patagonian Andes and into the foreland region at ~72-70°W.
238 The Don Juan Formation and Gastre dacites crop out farther east in the foreland domain.

239

240 3.3. *Intraplate volcanic units*

241

242 Two major intraplate volcanic provinces were emplaced during the Jurassic: (1) the
243 rhyolitic ignimbrites of the Marifil Formation which are exposed extensively along the Atlantic
244 margin (~185-167 Ma; Pankhurst and Rapela, 1995; Alric et al, 1996; Pankhurst et al, 2000); and
245 (2) the volcanic and volcanoclastic units of the NW-trending Cañadón Asfalto extensional basin,
246 these include the Cañadón Calcareo (~157 Ma), Cañadón Asfalto (~168-158 Ma), Lonco Trapial
247 (~180-172 Ma), and Las Leonares (~185-180 Ma) Formations (Cúneo et al, 2013; Hauser et al,
248 2017). Intraplate volcanic units of latest Cretaceous-Cenozoic age crop out across the modern
249 foreland region east of the North Patagonian Andes. These units include Late Cretaceous basalts
250 of the Tres Picos Prieto Formation (~80-62 Ma; Franchi and Page, 1980), the Paleocene-Eocene
251 Pilcaniyeu Belt (~60-42 Ma; Mazzoni et al, 1991; Wilf et al, 2010; Iannelli et al, 2017), and the
252 Oligocene-Miocene Somuncura Plateau (~33-16 Ma; Kay et al, 2007).

253

254 3.4. *Western versus eastern sediment source regions*

255

256 To investigate when the Andean hinterland became the dominant sediment source to the
257 retroarc region, we delineate two sediment source regions defined by the ~71°W boundary

258 between the North Patagonian Andes and the modern Patagonian broken foreland basin (Figs. 2
259 and 4).

260 In the west, the Andean domain includes the magmatic arc, fold-thrust belt, and pre-
261 Andean basemen, largely defined by rocks of the North Patagonian Batholith, Divisadero Group,
262 Lago la Plata Formation, and El Maitén Belt. On the eastern Andean flank, the Subcordilleran
263 Batholith and Devonian plutonic units intrude metamorphic units of the Paleozoic Colohuincul
264 Complex. On the western Andean flank, the Paleozoic accretionary complex hosts Devonian
265 intrusive rocks of the Chaitenia island arc terrane (~400–360 Ma; Hervé et al., 2013, 2016,
266 2018). A composite age distribution compiled from >740 published zircon U-Pb analyses (Fig.
267 4B) reveals a broad range of Precambrian to Jurassic age grains within pre-Andean basement.
268 Some of the most diagnostic age ranges from the North Patagonian Andes come from the North
269 Patagonian Batholith, with clusters of ~140-80 Ma and <20 Ma ages.

270 The eastern domain includes extensive intraplate volcanic units (Marifil Formation, Tres
271 Picos Prieto Formation, Pilcaniyeu Belt, Somuncura Plateau, Cañadón Asfalto Basin volcanic
272 rocks), North Patagonian massif basement units, and subordinate exposures of magmatic arc
273 units (Central Patagonian Batholith, Don Juan Formation, Gastre porphyritic rocks). Diagnostic
274 age ranges include early Pilcaniyeu volcanic rocks (~60-55 Ma) and the Marifil Formation
275 (~188-172 Ma). It is important to note that the Marifil Formation ignimbrite and plutonic
276 Subcordilleran Belt overlap in age. However, structural, thermochronologic, and shortening-
277 related growth stratal relationships indicate exhumation of the Andean fold-thrust belt during
278 middle-late Miocene time (Thomson et al., 2001; Giacosa and Heredia, 2004; Ramos et al, 2015;
279 Manuel López et al, 2019), suggesting the Subcordilleran Belt was not exposed as a potential
280 sediment source until Neogene time.

281

282 **4. Methods**

283

284 Fourteen fine- to medium-grained sandstone samples were collected from Cretaceous–
285 Neogene strata across the northern Chubut province of Argentina, mostly between 42 and 43°S,
286 from eastern (Lower Cretaceous), central (Upper Cretaceous), and western (Neogene) segments
287 of the Patagonian broken foreland (Table 1). All 14 sandstone samples were analyzed for detrital
288 zircon U-Pb geochronology and four of these were analyzed for Lu-Hf-Yb isotopic values (Figs.
289 2 and 3). Following conventional physical and chemical mineral density separation techniques
290 (including water table, heavy liquid and magnetic separation), a random selection of inclusion-
291 free zircon grains of variable size and shape were analyzed for U-Pb geochronology on the
292 Element2 HR ICPMS (inductively coupled plasma mass spectrometer), with subsequent Lu-Hf-
293 Yb isotope analyses on the Nu Plasma HR multicollector ICPMS at the University of Arizona
294 LaserChron Center. U-Pb and Lu-Hf-Yb analyses follow techniques defined by Gehrels et al.
295 (2006, 2008), Gehrels and Pecha (2014), and Cecil et al. (2011). We report U-Pb
296 geochronological results with measured age uncertainties of 1-2% (1σ error) and present results
297 for individual samples as maximum depositional ages (MDA; Fig. 5) and probability density
298 functions (Fig. 6). We use $^{206}\text{Pb}/^{238}\text{U}$ ages for zircons younger than 900 Ma and $^{206}\text{Pb}/^{207}\text{Pb}$ ages
299 for zircons older than 900 Ma. Individual analyses were filtered such that results displaying
300 >20% discordance, >5% reverse discordance, or 10% internal uncertainty were discarded. For
301 each sample, 100-125 individual zircon grain ages were obtained. MDAs for individual samples
302 are calculated on the basis of the youngest group of U-Pb ages, and reported as weighted mean
303 ages with 2σ analytical errors (Ludwig, 2008). In reporting MDAs, we consider the youngest

304 single grain, the youngest age peak, and the youngest population of grains overlapping at 2σ (>2-
305 3 grains) for each sample (Dickinson and Gehrels, 2009). Given the proximity of the Andean
306 magmatic arc, it is likely that some samples contain syndepositional volcanogenic zircons and
307 therefore some MDAs may represent approximations of the true depositional age (e.g.,
308 Dickinson and Gehrels, 2009; Horton et al., 2015; Schwartz et al., 2017; Daniels et al., 2018). Hf
309 isotopic results are reported in epsilon units (ϵ) and presented in Hf evolution diagrams (Fig. 7)
310 as $\epsilon\text{Hf}(t)$ values representing the isotopic composition at the time of crystallization (t) in
311 reference to CHUR (chondritic uniform reservoir; Bouvier et al., 2008), DM (depleted mantle;
312 Vervoort and Blichert-Toft, 1999) and average crustal evolution (assuming modern $^{176}\text{Lu}/^{177}\text{Hf} =$
313 0.0115 ; Vervoort and Patchett, 1996; Vervoort et al., 1999). Measured $^{176}\text{Hf}/^{177}\text{Hf}$ uncertainties
314 are ~ 1 epsilon unit (1ϵ). Detailed analytical methods, results, and supporting references are
315 provided in the supplementary material (Appendices A-C).

316

317 *4.1. Eastern segment: Lower to mid-Cretaceous samples*

318

319 The Aptian–Cenomanian Chubut Group is exposed only in the eastern segment of the
320 North Patagonian retroarc region (Figs. 2 and 3) and is evaluated here using new and published
321 U-Pb geochronological results. For the lower Chubut Group, a sample was collected from the
322 uppermost Los Adobes Formation near the Taquetrén Range (sample 17TQT03; $42^{\circ}57'25.02''\text{S}$,
323 $69^{\circ}13'15.07''\text{W}$). For the upper Chubut Group, Navarro et al. (2015) presented U-Pb results for
324 the undifferentiated Cerro Barcino Formation near Telsen (their samples SJS and TS2).

325

326 *4.2. Central segment: Upper Cretaceous samples*

327

328 In the central segment of the Patagonian broken foreland, the Upper Cretaceous-
329 Paleocene Paso del Sapo and Lefipán Formations (Figs. 2 and 3) are characterized by U-Pb
330 results for five samples, listed here in stratigraphic order. Two samples were collected from
331 some of the only exposures of the basal Paso del Sapo Formation, which locally overlies the
332 Jurassic Lonco Trapial Formation in the central outcrop belt along the Chubut River (sample
333 17PDS04: 42°40'54.12"S, 69°45'4.57"W) and eastern outcrop belt in the Taquetrén Range
334 (sample 17TQT01; 42°55'7.00"S, 69°15'2.22"W). An additional sample from the Taquetrén
335 Range was presented by Echaurren et al. (2016) for interpreted Paso del Sapo growth strata
336 associated with initial shortening in the region (their sample PS-01). Samples from the transition
337 from the uppermost Paso del Sapo (17PDS19) to lowermost Lefipán Formation (17PDS20) along
338 the Chubut River (42°40'9.12"S, 69°51'22.73"W) were collected from a stratigraphic section
339 described by Spalletti (1996) and Scasso et al. (2012).

340

341 4.3. Western segment: Neogene samples

342

343 Neogene deposits of the Collón Curá and Ñirihuau Formations are most prevalent where
344 collected in western segments of the Patagonian broken foreland basin and the adjacent foothills
345 of the North Patagonian Andes (Figs. 2 and 3). Samples from the lowermost Neogene levels
346 were collected from outcrops considered to be the lower Ñirihuau Formation, which directly
347 overlying upper Eocene-Oligocene volcanic rocks in the Esquel Range (17ESQ01:
348 42°51'21.20"S, 71°20'11.98"W) and the El Maitén Belt (17CUS02 and 17CUS03: 42°4'16.61"S,
349 71°1'32.70"W) of the Andean foothills. From higher stratigraphic levels, samples from separate

350 growth stratal packages (Fig. 8) include the upper Ñirihuau Formation associated with uplift of
351 the Esquel Range (17ESQ02 and 17ESQ03: 42°59'6.29"S, 71°29'21.77"W) (Echaurren et al.,
352 2016) and the Collón Curá Formation associated with uplift of the Cordón del Maitén near the
353 town of Cushamen (17CUS04 and 17CUS5: 42° 5'51.14"S, 70°55'11.28"W) (Ramos et al., 2015;
354 their samples 13-M2, MR-2, and 13-M4). The lower levels of the regionally extensive Collón
355 Curá Formation were sampled in the west near the Tecka Range (17TEC01: 43°23'32.89"S,
356 70°44'27.85"W) and farther east along the Chubut River near the town of Paso del Sapo
357 (17PDS02: 42°40'59.27"S, 69°39'41.40"W; locally La Pava Formation) where it disconformably
358 overlies the Upper Cretaceous Paso del Sapo Formation.

359

360 **5. Detrital zircon U-Pb geochronological results and interpretations**

361

362 Sediment provenance patterns and depositional ages for the Patagonian broken foreland
363 basin (Figs. 2 and 3) are assessed using U-Pb geochronological results for the Lower Cretaceous
364 through Neogene succession (Appendices A-C). The results help refine chronostratigraphic age
365 estimates (Fig. 5), identify sediment source regions and changes in sediment routing (Fig. 6),
366 clarify crustal evolution patterns (Fig. 7), and define the age of key growth structures (Fig. 8).

367

368 *5.1. Refined chronostratigraphy and depositional ages*

369

370 New estimates of maximum depositional age (MDA) are presented for 8 samples from
371 the Cretaceous-Paleogene succession (Fig. 5). The results are summarized here in approximate

372 stratigraphic order for western, central, and eastern segments of the broken foreland region
373 (Table 2; Figs. 2 and 3).

374 For the Cretaceous-Paleocene succession in the central to eastern basin segments, the
375 upper Los Adobes Formation (lower Chubut Group) produced a single youngest grain of Albian
376 age (106.9 ± 2.2 Ma), with no additional grain ages overlapping within error. Results for the
377 Cerro Barcino Formation presented by Navarro et al. (2015; samples SJS and T2S) also contain
378 Albian grains, with MDAs of 107 ± 4.3 Ma and 112 ± 11 Ma. The basal Paso del Sapo
379 Formation yields an MDA of 72.1 ± 1.6 Ma (sample 17PDS04; n=2 grains), in accordance with
380 ages of 71.0 ± 2.4 Ma and 71.9 ± 1.8 Ma for the single youngest grains for two additional
381 samples from the Paso del Sapo Formation (17PDS04, 17PDF19). These latest Campanian-
382 Maastrichtian ages all overlap within error and are considerably younger than a previously
383 reported MDA near the Santonian-Campanian boundary of 83.1 ± 1.6 Ma (Echaurren et al.,
384 2016; sample PS-01). Upsection, the overlying Maastrichtian-lower Paleocene Lefipán
385 Formation contains a youngest grain (81.4 ± 1.8 Ma) older than the aforementioned youngest
386 grains from the underlying Paso del Sapo Formation.

387 Within the Neogene succession, which is best expressed in the Andean foothills and
388 western foreland, new MDAs clarify the depositional ages of the Ñirihuau and Collón Curá
389 Formations (Fig. 5). In the El Maitén belt, a sample from the oldest basin fill provides an MDA
390 of 22.2 ± 0.3 Ma (sample 17CUS3). This sample is from a basal exposure of a clastic succession
391 that directly overlies the late Eocene-Oligocene volcanic rocks of the Ventanta Formation. The
392 early Miocene MDA indicates deposition of the basal Ñirihuau Formation partially coeval with
393 late El Maitén magmatism (~ 22 Ma). In the Andean foothills, near Esquel, 3 samples from the
394 better-studied exposures of Ñirihuau Formation yield MDAs, in stratigraphic order, of 16.9 ± 0.1

395 Ma, 13.1 ± 0.2 Ma, and 12.5 ± 0.3 Ma (samples 17ESQ01, 17ESC02, and 17ESQ03,
396 respectively). The Collón Curá Formation is rich in volcanogenic materials and shows
397 comparable MDAs of 14.7 ± 0.2 Ma and 14.6 ± 0.4 for samples from lower levels in the central
398 (17TEC01) and eastern (17PDS02) basin segments. In the central zone, samples from
399 successively higher levels display an MDA of 10.1 ± 0.2 Ma (17CUS04) followed by a single
400 grain age of 9.3 ± 0.3 Ma (17CUS5).

401

402 5.2. Sediment provenance results

403

404 Consideration of detrital zircon U-Pb results for all 17 samples, as depicted in a
405 composite probability density plot (Fig. 6), helps delineate 8 major age populations within the
406 Cretaceous-Cenozoic Patagonian broken foreland: ~410–360 Ma, ~330–280 Ma, ~230–210 Ma,
407 ~200–170 Ma, ~140–80 Ma, ~60–50 Ma, ~40–30 Ma and ~20–10 Ma. Five of these populations
408 can be assigned to discrete sediment source units, including three major western sources in the
409 North Patagonian Batholith (~140–80 Ma; <20 Ma), Subcordilleran Batholith (~185–180 Ma),
410 and El Maitén Belt (~37–20 Ma), and two major eastern sources in the Marifil Formation (~188–
411 172 Ma) and Pilcaniyeu Belt (~60–42 Ma). The original sources for pre-Jurassic age populations
412 are more ambiguous, as these ages may have originated from similar Paleozoic crystalline rocks
413 of pre-Andean basement in the west or the North Patagonian Massif in the east (Fig. 4b).

414

415 5.2.1. Lower to mid-Cretaceous strata

416 For the Lower Cretaceous Chubut Group, 3 samples contain nearly unimodal U-Pb age
417 distributions dominated by Middle Jurassic (200–180 Ma) ages and limited mid-Cretaceous

418 (110–100 Ma) ages (Fig. 6). We interpret the vast majority of these sediments to have been
419 derived from the Marifil Formation in distal eastern regions (Figs. 2 and 4). Navarro et al.
420 (2015) document west-directed paleoflow within the Chubut Group, consistent with a major
421 source in the east. However, minor contributions of mid-Cretaceous ages can only come from
422 young or syndepositional igneous materials linked to arc magmatism associated with the North
423 Patagonian Batholith to the west. A sample from the Los Adobes Formation (17TQT03) also
424 contains significant Permian and Devonian populations. The Paleozoic-age zircons in the Los
425 Adobes Formation are potentially sourced from nearby granitic basement units of the North
426 Patagonian Massif (including the Mamil Choique and Paso del Sapo granites, and San Martín
427 tonalite).

428

429 *5.2.2. Upper Cretaceous strata*

430 For the Upper Cretaceous to lower Paleocene Paso del Sapo and Lefipán Formations, 5
431 samples exhibit markedly uniform detrital zircon U-Pb age distributions (Fig. 6). In each
432 sample, a group of mid- to Late Cretaceous grains (130–80 Ma) is dominant and provides a clear
433 signal of derivation from Andean sources in the North Patagonian Batholith (Figs. 2 and 4).
434 Although limited, possibly syndepositional zircon grains (Fig. 5) suggest additional input from
435 active volcanic sources in the Andean magmatic arc. A subordinate group of Paleozoic ages
436 spanning from roughly 400 to 300 Ma can be tied to sources of Devonian intrusive rocks and
437 associated host rocks (Colohuincul Complex) along the eastern flank of the Andes (Hervé et al.,
438 2013, 2016, 2018). We interpret Upper Cretaceous basin fill as derived entirely from western
439 sources during initial growth of the North Patagonian Andes. The Late Cretaceous shift in

440 provenance represents a basin-wide reversal in sediment polarity (Horton, 2018a), with a switch
441 from eastern to western sources.

442

443 5.2.3. Neogene strata

444 Nine samples from various segments of Neogene basin fill yield the most varied U-Pb
445 results with cosmopolitan age distributions (Fig. 6). Although there are variations among
446 samples, most age groups can be linked to (1) the Early Jurassic Subcordilleran Batholith, (2) the
447 Cretaceous North Patagonian Batholith, (3) Paleogene intraforeland volcanic belts, and (4) the
448 Neogene Andean magmatic arc.

449 The lowermost levels of Neogene basin fill are characterized by two samples from clastic
450 deposits considered to be the basal Ñirihuau Formation; these samples (17CUS2 and 17CUS3)
451 are dominated by Early Jurassic grains (190-180 Ma) likely derived from the Subcordilleran
452 Batholith, which is involved in the North Patagonian fold-thrust belt at these latitudes (Fig. 2). A
453 subordinate late Paleocene population is unique to the Pilcaniyeu Belt (~60-42 Ma, Huitrera
454 Formation). An upsection introduction of Oligocene to early Miocene ages is representative of
455 the El Maitén Belt directly to the west. The youngest U-Pb ages (Fig. 5) are considered the
456 products of syndepositional arc magmatism related to igneous activity in the North Patagonian
457 Batholith. A broad range of roughly 400-280 Ma ages can be linked to the Colohuincul
458 Complex and associated Devonian intrusions. Alternatively, these Paleozoic ages could be
459 derived from the Paleozoic Accretionary Complex along the western Andean flank.

460 Three samples from the western exposures of the Ñirihuau Formation in the North
461 Patagonian Andes near Esquel (samples 17ESQ01, 17ESQ02, 17ESQ03) record enhanced
462 proportions of Paleozoic (380-270 Ma) ages, Cretaceous (120-80 Ma) ages, and syndepositional

463 Miocene (<20 Ma) ages (Fig. 6), which are attributed individually to derivation from pre-Andean
464 bedrock (Colohuincul Complex and Devonian intrusions), the North Patagonian Batholith, and
465 the active magmatic arc, respectively. All of these age groups are restricted to western source
466 regions. Progressive upsection younging of Miocene arc-derived ages attests to continued input
467 from a contemporaneous magmatic arc. Additional upsection trends include increases in Jurassic
468 (Subcordilleran Belt) and Paleozoic (pre-Andean basement) ages, and the limited appearance of
469 late Paleocene-early Eocene ages potentially derived from the Pilcaniyeu Belt.

470 The U-Pb results from four samples of the Collón Curá Formation show similar age
471 signatures as the Ñirihuau Formation but in different proportions (Fig. 6). A continuous
472 presence of Miocene grains, including syndepositional grains (Fig. 5), attests to steady volcanic
473 input from the Andean magmatic arc. Additional age groups include Cretaceous (120-80 Ma)
474 ages diagnostic of the North Patagonian Batholith, Jurassic ages from the Subcordilleran
475 Batholith, and Paleozoic ages from pre-Andean units. Two samples from the easternmost Collón
476 Curá Formation (17TEC01 and 17PDS02) are notable for the absence of Cretaceous grains,
477 potentially the product of eastward downstream dilution by additional source materials. One of
478 these samples (17PDS02) is further distinguished by a unique Triassic (250-210 Ma) group that
479 is not observed in any other detrital samples in this study. This population is likely derived from
480 intraforeland sources diagnostic of the North Patagonian Massif (Central Patagonian Batholith,
481 Mamil Choique granite and equivalents).

482 Two samples from higher levels of the Collón Curá Formation, from a growth stratal
483 succession near El Maitén (17CUS04 and 17CUS05) (Fig. 8), display perhaps the most diverse
484 age distributions of any samples in the broken foreland (Fig. 6). These samples contain
485 Paleozoic, Early Jurassic, Cretaceous, Paleogene, and Neogene age groups. Most of these

486 signatures are consistent with derivation from rock units within the North Patagonian fold-thrust
487 belt and Neogene magmatic arc to the west, similar to the Ñirihau Formation, with the
488 exception of Paleocene-Eocene ages likely derived from intraforeland sources of the volcanic
489 Pilcaniyeu Belt to the north or east.

490

491 5.3. Age of growth strata

492

493 Several additional constraints arise from consideration of U-Pb results and MDAs for
494 synorogenic basin fill associated with shortening in the fold-thrust belt and broken foreland of
495 northern Patagonia. We highlight three cases where growth stratal relationships allow
496 determination of the timing of activity along particular contractional structures (Table 2). These
497 examples include the frontal segment of the fold-thrust belt in the North Patagonian Andes and
498 the proximal (western) and distal (eastern) sectors of the broken foreland basin.

499 An early phase of retroarc deformation in the distal foreland is supported by U-Pb results
500 for basin fill associated with a growth structure along the flank of the Taquetrén Range, a
501 basement-involved uplift ~120-150 km east of the modern Andean mountain front (Fig. 2).
502 Echaurren et al. (2016) described growth strata in the Upper Cretaceous Paso del Sapo
503 Formation in the footwall of the southwest-directed Taquetrén thrust. From these deposits,
504 Echaurren et al. (2016) obtained a MDA of 83.1 ± 1.6 Ma (their sample PS-01). Results
505 presented here for three additional samples of the Paso del Sapo Formation farther west of the
506 Taquetrén thrust show tightly clustered MDAs and single youngest grains of 72.1 ± 1.6 Ma, 71.9
507 ± 1.8 Ma, and 70.9 ± 1.4 Ma (17PDS04, 17PDS19, and 17TQT01). Two of these samples were
508 collected from the basal Paso del Sapo Formation (17PDS04 and 17TQT01) approximately 40

509 km apart (Fig. 2); for this reason we interpret a late Campanian-Maastrichtian age of deposition
510 and contemporaneous thrusting and structural partitioning of the Cretaceous foreland basin.

511 In the foothills of the North Patagonian Andes, growth strata within the Ñirihuau
512 Formation (Fig. 8A; Echaurren et al., 2016) are associated with motion along an east-directed
513 thrust structure responsible for uplift of the Esquel Range, a prominent north-trending range
514 within the frontal (eastern) segment of the fold-thrust belt (Fig. 2). Samples from pre-growth
515 and overlying growth strata yield MDAs of 13.1 ± 0.2 Ma and 12.5 ± 0.3 Ma (samples 17ESC02
516 and 17ESQO3) (Fig. 5). These ages indicate continuous deposition with no major hiatus during
517 middle Miocene shortening in this foothills segment of the fold-thrust belt.

518 Farther east, younger growth strata within the Collón Curá Formation (Fig. 8B),
519 identified by Ramos et al. (2015), can be linked to motion along a blind east-directed fold-thrust
520 structure within the broken foreland region. Samples from pre-growth and overlying growth
521 strata display youngest U-Pb ages of 10.1 ± 0.2 Ma and 9.3 ± 0.3 Ma (samples 17CUS04 and
522 17CUS05), respectively. These U-Pb results are slightly younger than previously reported ages
523 of 13.5 to 11.3 Ma (Ramos et al., 2015; their samples 13-M2, MR-2, and 13-M4). These timing
524 constraints demonstrate a late Miocene phase of shortening and further compartmentalization of
525 the broken foreland basin. This deformation can be attributed to contractional structures
526 responsible for uplift of the Cordón del Maitén, a north-trending range constructed during
527 Neogene inversion of older normal faults, which originally formed during late Eocene-Oligocene
528 extension within the El Maitén Belt and associated emplacement of widespread ignimbrites of
529 the Ventana Formation.

530

531 **6. Hf isotopic results and interpretations in the context of arc magmatism**

532

533 From the detrital zircon samples, 4 samples (17PDS04, 17TQT01, 17CUS02, 17ESQ01)
534 were selected for Hf isotope analyses in order to assess Mesozoic-Cenozoic crustal evolution and
535 magmatic patterns from 200 to 10 Ma (e.g., Pepper et al., 2015; Balgord, 2017). A total of 130
536 new analyses are combined with 43 published Hf isotopic results from samples of sandstones
537 (Hauser et al., 2017) and 26 modern river sand results (Pepper et al., 2015) into a single Hf
538 evolution diagram (Fig. 7). The isotopic results include $\epsilon\text{Hf}(t)$ values ranging from -20 to +14
539 with individual mean values (for a given age) ranging from -8 to +8.

540 Consideration of a composite U-Pb age distribution (Fig. 7B) allows discrimination of 5
541 dominant age groups and corresponding Hf values: (1) 200–150 Ma, $\epsilon\text{Hf}(t) = -17$ –8 range (-8–2
542 mean); (2) 140–70 Ma, $\epsilon\text{Hf}(t) = -22$ –14 range (2–7 mean); (3) 60–42 Ma, $\epsilon\text{Hf}(t) = -5$ –7 range
543 (2–5 mean); (4) 40–20 Ma, $\epsilon\text{Hf}(t) = -7$ –12 range (5–8 mean); and (5) 20–9 Ma, $\epsilon\text{Hf}(t) = -13$ –10
544 range (3–7 mean). These results highlight the Hf isotopic signatures of key magmatic units,
545 including the North Patagonian Batholith, El Maitén Belt, Pilcanyeu Belt, Lonco Trapial
546 Formation (Cañadon Asfalto Basin), and Marifil Formation. These intrusive and extrusive units
547 have diverse magmatic affinities (subduction-related, intraplate and intermediate) related to
548 variable tectonic regimes (extension and shortening).

549 These records can then be compared with associated transitions in Andean magmatic arc
550 behavior (arc advance, cessation, and retreat), on the basis of a new compilation of published
551 isotopic ages of arc magmatism (Fig. 9). Here we highlight several key observations in the Hf
552 isotopic record of crustal evolution (Fig. 7) and the time-space history of arc magmatism (Fig. 9),
553 and then consider how these results support previous interpretations of the regional tectonic
554 evolution of northern Patagonia.

555 (1) For the Jurassic age group, a clear trend from moderately negative to positive epsilon
556 Hf signatures ($\epsilon\text{Hf}(t) = 17\text{--}8$ range; $-8\text{--}2$ mean) indicate progressively more juvenile magmatic
557 contributions from ~ 200 to 150 Ma (Fig. 7). This broadly coincided with a prolonged period of
558 extension from the latest Triassic to earliest Cretaceous ($\sim 210\text{--}140$ Ma; Rapela and Pankhurst,
559 1992; Folguera and Iannizzotto, 2004; Figari, 2005; Ramos, 2009) accompanied by Jurassic
560 phases of intraplate to intermediate magmatism reflected in $\sim 188\text{--}178$ Ma lower crustal melts of
561 the Marifil Formation and $\sim 190\text{--}157$ Ma intermediate volcanic rocks of the Lonco Trapial
562 Formation in the Cañadon Asfalto Basin (Pankhurst et al., 2000; Zaffarana et al., 2012, 2014).
563 Navarrete et al. (2016) proposed that the overall extensional tectonic regime was punctuated by
564 brief episodes of shortening ($\sim 188\text{--}185$, $\sim 170\text{--}163$, $\sim 157\text{--}136$ Ma). We interpret the Jurassic
565 trend toward increasingly positive Hf values to reflect progressively greater degrees of mantle
566 derivation during continued crustal extension.

567 (2) Hf isotopic data for the Cretaceous age group ($\sim 140\text{--}70$ Ma) show a broad
568 distribution of values ($\epsilon\text{Hf}(t) = -22\text{--}14$ range; $2\text{--}7$ mean), with mostly positive (juvenile) values
569 but an important subset of negative values indicative of considerable variation and locally
570 evolved signatures (Fig. 7). The negative values are concentrated in the $120\text{--}90$ Ma range,
571 coincident with estimates for a late Early Cretaceous onset of shortening in northern Patagonia
572 (Suárez et al., 2009b, 2010; Navarro et al., 2015; Echaurren et al., 2016). The Cretaceous also
573 marks the main phase of subduction-related arc magmatism in the North Patagonian Batholith
574 ($\sim 135\text{--}80$ Ma, Pankhurst et al., 1999; Suárez and del la Cruz, 2001). We interpret these results as
575 the products of initial Andean shortening and spatially irregular thickening of a previously
576 thinned continental crust and lithosphere. A possible weak trend toward higher Hf values until
577 ~ 90 Ma was followed by a restricted range of relatively more negative values, coeval with a Late

578 Cretaceous phase of eastward inboard advance of the magmatic arc toward the foreland (Fig. 9),
579 the probable result of slab flattening (Pankhurst et al., 1999; Echaurren et al., 2016, 2017).

580 (3) During the latest Cretaceous, a decrease in Hf isotopic values ($\epsilon\text{Hf}(t) = -5$ – -7 range; 2–
581 5 mean) immediately followed the eastward advance of the Andean magmatic arc and coincided
582 with an apparent cessation of arc magmatism (~ 75 – 50 Ma; Figs. 7 and 9). Thereafter, a
583 continued decrease in Hf values is expressed as Paleocene-Eocene bimodal intraplate
584 magmatism of the Pilcaniyeu Belt (~ 60 – 42 Ma; Iannelli et al., 2017). The Hf trend is consistent
585 with relatively more evolved signatures due to greater crustal contributions, which may reflect
586 interactions with a thickened crust generated during Late Cretaceous shortening.

587 (4) A mid-Cenozoic shift to increasingly positive Hf values ($\epsilon\text{Hf}(t) = -7$ – -12 range; 5–8
588 mean) in the 40–20 Ma time window (Fig. 7) was contemporaneous with a late Eocene–early
589 Miocene phase of minor to moderate extension (Rapela et al., 1988; Orts et al., 2012) and
590 associated volcanism in the El Maitén Belt (~ 37 – 20 Ma; Fernández Paz, 2018; Bechis et al.,
591 2014). Although the magnitude of extension within the overriding plate is poorly constrained,
592 we interpret this trend toward more juvenile isotopic signatures as the product of crustal thinning
593 and greater mantle input during probable slab rollback (Horton, 2018b).

594 (5) During the Miocene, over the ~ 20 – 9 Ma time frame, broadly distributed Hf isotopic
595 values ($\epsilon\text{Hf}(t) = -13$ – -10 range; 1–7 mean) display a pronounced shift to lower values (Fig. 7).
596 This signature is synchronous with the main phase of Andean shortening commencing at ~ 20 Ma
597 (Giacosa and Heredia, 2004; Ramos et al., 2015; Echaurren et al., 2016), as well as renewed arc
598 magmatism within the North Patagonian Batholith (< 20 Ma; Aragon et al. 2011b). The more
599 evolved signatures are consistent with Neogene crustal thickening and greater crustal interactions

600 during enhanced magmatism. This final phase potentially coincided with arc retreat, with an
601 apparent westward broadening of the Andean magmatic arc (Fig. 9).

602

603 **7. Discussion**

604

605 Accurate determinations of depositional ages and sediment provenance from detrital
606 zircon U-Pb geochronological analyses help constrain the regional chronostratigraphic
607 framework, timing of deformation, duration of depositional hiatuses, and inception of foreland
608 basin sedimentation in northern Patagonia within the northern Chubut province of Argentina (42-
609 43°S; Figs. 3, 5, and 6). A compilation of published isotopic ages demonstrates distinctive
610 western and eastern source regions during Cretaceous–Miocene evolution of the Patagonian
611 broken foreland basin (Fig. 4). In addition, new Hf isotopic results (Fig. 7), a synthesis of
612 published magmatic ages (Fig. 9), and consideration of magmatic affinities and deformational
613 modes within the overriding plate facilitate an evaluation of magmatic arc behavior and
614 continental crustal evolution (Fig. 10).

615

616 *7.1. Stratigraphic ages for the Patagonian broken foreland*

617

618 The depositional ages of basin-fill units and duration of stratigraphic hiatuses are not
619 fully resolved for the North Patagonian retroarc region. New and published detrital zircon U-Pb
620 results indicate periods of sediment accumulation in the Aptian-Cenomanian (~106–97 Ma;
621 Chubut Group), Campanian–early Paleocene (~74–62 Ma; Paso del Sapo and Lefipán
622 Formations), and Miocene (~22–9 Ma; Ñirihuau, La Pava, and Collón Curá Formations), with

623 intervening hiatuses in the Late Cretaceous (~97–74 Ma) and the late Paleocene–Oligocene
624 (~62–22 Ma; Figs. 3 and 5).

625

626 *7.2. Reversal in sediment polarity*

627

628 The onset of Andean mountain building and flexural foreland subsidence can be linked to
629 major drainage reorganization and a switch to orogenic sediment provenance (Horton, 2018a).
630 In northern Patagonia, Jurassic to Lower Cretaceous deposits are uniformly derived from eastern
631 sources in the North Patagonian Massif, principally from volcanic rocks of the Marifil Formation
632 (Fig. 6), consistent with paleoflow from the east as determined by Navarro et al (2015). A
633 Campanian–Maastrichtian switch to western orogenic sources is recognized in the Paso del Sapo
634 Formation, with nearly exclusive derivation from the North Patagonian Batholith and associated
635 pre-Andean basement (Fig. 10), supported by paleoflow from the west documented by Spalletti
636 (1996) and Scasso et al (2012). This Late Cretaceous reversal in sediment polarity was coeval
637 with a period of shortening and eastward advance of the magmatic arc during flat-slab
638 subduction (Fig. 9). Sediment routing systems derived from western sources in the Andes
639 persisted into the Neogene with dominance by the Cretaceous–Cenozoic North Patagonian
640 Batholith, Jurassic Subcordilleran Batholith, and Paleozoic pre-Andean basement (Fig. 6).
641 Neogene units show subordinate input from intraplate volcanic rocks to the east (Pilcaniyeu
642 Belt), as most sediment delivered to the basin was linked to shortening-induced exhumation in
643 the Andean fold-thrust belt and broken foreland.

644

645 *7.3. Deformation timing from synorogenic growth strata*

646

647 Cretaceous-Cenozoic growth strata associated with upper crustal structures constrain the
648 timing of shortening in the Patagonian broken foreland (Fig. 10). These synorogenic deposits are
649 associated with growth and eastward propagation of the fold-thrust belt and reactivation of
650 inherited Jurassic normal faults, which localized basement-involved shortening in the foreland
651 (e.g., Bilmes et al., 2013; Ramos et al., 2015; Echaurren et al., 2016). New chronostratigraphic
652 constraints from detrital zircon U-Pb geochronology help constrain structural timing for three
653 major growth stratal successions (Figs. 2, 5, and 8). Although Cretaceous deposits in the Andes
654 are commonly linked to post-extensional thermal processes and the generation of regional sag
655 basins (e.g., Uliana et al., 1989), reported growth strata within the Los Adobes and Paso del Sapo
656 formations have been associated with reactivation of a Jurassic normal fault and uplift of pre-
657 Jurassic basement that produced the Taquetrén Range, indicative of initial Andean shortening
658 during Aptian(?)–Albian to Maastrichtian time (Echaurren et al., 2016).

659 For the Cenozoic succession, new depositional age constraints for pre-growth and growth
660 strata refine deformational timing of contractional structures in the frontal thrust-belt foothills
661 (Esquel Range) and proximal foreland (El Maitén Range; Ramos et al., 2011; 2015; Bilmes et
662 al., 2013; Orts et al., 2012; Echaurren et al., 2016). Middle Miocene growth strata in the
663 Ñirihuau Formation (samples 17ESQ01, 17ESQ02, and 17ESQ03) suggest that shortening in the
664 frontal segment of the fold-thrust belt and corresponding uplift of the Esquel Range had
665 commenced by ~13–12 Ma (Fig. 8A). Farther east, upper Miocene growth strata in the Collón
666 Curá Formation (samples 17CUS04 and 17CUS05) suggests that shortening-related growth of
667 the Cordón del Maitén (including possible reactivation of mid-Cenozoic extensional structures
668 and further partitioning of the broken foreland basin) was underway at 10–9 Ma (Fig. 8B). The

669 growth stratal relations are in accordance with available low-temperature thermochronological
670 data, which demonstrate exhumation-related Late Cretaceous-Paleogene cooling in the broken
671 foreland and late Miocene-Pliocene cooling along the frontal fold-thrust belt (Savignano et al.,
672 2016).

673

674 *7.4. Crustal evolution and magmatism*

675

676 The retroarc region of northern Patagonia recorded a complex history of varying
677 deformational mode (shortening and extension), magmatism of diverse affinities (subduction-
678 related, intraplate, and intermediate), and Andean magmatic arc behavior (advance/expansion,
679 cessation, and rejuvenation) (Figs. 9 and 10). Hf isotopic results elucidate crustal evolution
680 trends that can be evaluated in the context of magmatic affinity and tectonic regime (Fig. 7).

681

682 *7.4.1. Arc magmatism*

683 Late Cretaceous broadening and eastward advance of the subduction-related magmatic
684 arc (Figs. 9 and 10) was followed by Paleogene arc cessation in northern Patagonia (Folguera
685 and Ramos, 2011; Gianni et al., 2018). A compilation of ~160 published magmatic arc ages at
686 ~40-46°S support this assertion (Fig. 9; see earlier synthesis by Gianni et al., 2018). Arc
687 broadening toward the foreland appears to have occurred at ~90–70 Ma, followed by a ~70–55
688 Ma period of arc shutoff. Renewed arc magmatism for the remainder of the Cenozoic and
689 possible westward retreat occurred from ~55 to 10 Ma. Time-space variations in arc magmatism
690 suggest a Late Cretaceous-Paleogene phase of slab shallowing (possibly to a flat-slab
691 configuration) followed by slab resteepeening during Eocene-Oligocene time (Suárez and de la

692 Cruz, 2001; Folugera and Ramos, 2011). Such transitions in subducting slab dynamics may
693 correlate with phases of foreland partitioning through the activation of basement-involved
694 structures (e.g., Echaurren et al., 2016; Savignano et al., 2016; Gianni et al., 2018). Moreover,
695 arc quiescence was partially coeval with the proposed Paleocene collision of the Farallon-Aluk
696 ridge south of 43°30'S (Cande et al., 1986; Ramos, 2005; Aragón et al., 2011b). Mid-Cenozoic
697 renewal of arc magmatism was followed by enhanced Miocene arc magmatism in the North
698 Patagonian Batholith, roughly coincident with plate reorganization involving breakup of the
699 Farallon plate and subduction of the Nazca plate at ~23 Ma (Kay et al., 2007). The availability
700 of published isotopic ages influences these interpreted patterns of arc magmatism, with particular
701 concern over the relatively sparse sampling of more-eastern regions and Late Cretaceous
702 magmatic units (Fig. 9).

703

704 7.4.2. *Crustal evolution*

705 To elucidate trends in crustal evolution since ~200 Ma, individual and running mean
706 values are considered for >200 Hf isotopic results (Fig. 7), with 130 analyses from this study and
707 >70 from published datasets. Five Mesozoic-Cenozoic phases are identified (Fig. 7A, gray
708 arrows) on the basis of shifts in Hf signatures. More negative epsilon Hf values correspond to
709 more evolved crustal signatures and more positive epsilon Hf values indicate less evolved (more
710 juvenile) signatures. Despite a complex history of varying deformational mode, magmatism of
711 divergent affinities, and Andean magmatic arc behavior (Fig. 9), the identified Hf isotopic trends
712 in crustal evolution (Fig. 7) appear to highlight several key transitions in tectonic setting (Fig.
713 10). (1) Phases of extension in both Jurassic (200-150 Ma) and mid-Cenozoic (40-20 Ma)
714 produce more juvenile trajectories despite divergent magmatic affinities. (2) Phases of

715 shortening in both the Cretaceous (120-90 Ma) and Neogene (<20 Ma) generated more evolved
716 values emblematic of crustal thickening. (3) Important transitions in crustal evolution may also
717 be related to a range of processes—slab shallowing, flat-slab subduction, slab resteepeening, ridge
718 collision (and slab-window formation), and oceanic plate breakup—in operation sequentially
719 during latest Cretaceous-Paleogene evolution of northern Patagonia.

720

721 **8. Conclusions**

722

723 New U-Pb and Hf isotopic results help define the chronostratigraphic framework,
724 sediment provenance history, and crustal evolution patterns for the Patagonian broken foreland
725 basin during geodynamic transitions in overriding plate deformational mode (shortening versus
726 extension) and variations in subduction-related arc magmatism (advance, retreat, cessation, and
727 rejuvenation). Detrital zircon U-Pb geochronological data help constrain the depositional ages of
728 Cretaceous-Neogene strata, including Upper Cretaceous and Miocene growth strata linked to
729 shortening in the fold-thrust belt (North Patagonian Andes) and to intraforeland basement uplifts
730 (Taquetrén Range) which likely reactivate preexisting structural elements. U-Pb results also
731 facilitate the discrimination of sediment provenance in terms of Andean sources to the west
732 (North Patagonian Batholith, Subcordilleran Batholith, and pre-Andean basement) versus
733 platformal sources to the east (North Patagonian Massif and intraplate volcanic units). Whereas
734 initial retroarc deposits were originally fed by eastern sources (Chubut Group), a Late Cretaceous
735 reversal in sedimentary polarity is defined by the nearly exclusive derivation of Campanian-
736 Maastrichtian and younger sediments (Paso del Sapo Formation and overlying clastic strata)
737 from the Andean magmatic arc and orogenic belt to the west.

738 The Patagonian broken foreland provides a detrital record of key tectonic events in the
739 northern Chubut province of Argentina. Eastward advance of the Andean magmatic arc at ~90–
740 70 Ma and subsequent shutoff at ~70–55 Ma is consistent with slab shallowing and subsequent
741 flat-slab subduction. Thereafter, slab rollback coincided with a late Eocene–early Miocene phase
742 of extension and related magmatism (El Maitén Belt) and long hiatus in foreland basin
743 sedimentation. The Neogene depositional record (Ñirihuau and Collón Curá Formations) was
744 governed by upper crustal shortening, renewed arc magmatism, and accumulation of clastic basin
745 fill associated with contractional structures in the foothills of the fold-thrust belt and broken
746 foreland farther east. The Mesozoic-Cenozoic history of variable contractional and extensional
747 tectonic regimes is largely reflected in ϵHf signatures that recorded contrasting evolved and
748 juvenile signatures during crustal thickening and thinning, respectively.

749

750 **Acknowledgements**

751

752 This research was funded by the U.S. National Science Foundation (Graduate Research
753 Fellowship to Butler and grant EAR 1348031 to Horton), and research grants (to Butler) from the
754 Geological Society of America, American Association of Petroleum Geologists, SEPM (Society
755 for Sedimentary Geology), and the Jackson School of Geosciences at the University of Texas at
756 Austin. We thank Peter Flaig for field assistance, and Sarah George, Lily Jackson, Tomas
757 Capaldi, Chelsea Mackaman-Lofland and Gabriel Giacomone for valuable discussions.
758 Constructive reviews from Theresa Schwartz and Andrés Bilmes improved the manuscript.

759

760

761

762

763 **Supplementary data**

764 *Appendix A. U-Pb geochronology methods*

765

766 *Appendix B. Zircon U-Pb isotopic results*

767

768 *Appendix C. Zircon Lu-Hf isotopic results*

769

770

ACCEPTED MANUSCRIPT

771 **References**

- 772
- 773 Adriasola, A.C., Thomson, S.N., Brix, M.R., Hervé, F., Stöckhert, B., 2005. Postmagmatic
774 cooling and late Cenozoic denudation of the North Patagonian Batholith in the Los Lagos
775 region of Chile, 41°- 42°15S. *Int. J. Earth Sci.* 95, 504-528.
- 776 Alric, V., 1996. Los basaltos portadores de xenolitos aflorantes en las localidades Paso de Indios
777 y cerro Cóndor, departamento de Paso de Indios, Provincia del Chubut. Doctoral Thesis.
778 Universidad Nacional de la Patagonia San Juan Bosco, 135.
- 779 Aragón, E., Castro, A., Díaz-Alvarado, J, Liu, D.Y., 2011a. The North Patagonian batholith at
780 Paso Puyehue (Argentina-Chile). SHRIMP ages and compositional features. *J. S. Am.*
781 *Earth Sci.* 32, 547-554.
- 782 Aragón, E., D'Eramo, F., Castro, A., Pinotti, L., Brunelli, O.S., Rivalenti, G., Varela, R.,
783 Spakman, W., Demartis, M., Cavarozzi, C.E., Aguilera, Y.E., Mazzucchelli, M., Ribot,
784 A., 2011b. Tectono-magmatic response to major convergence changes in the North
785 Patagonian suprasubduction system; the Paleogene subduction–transcurrent plate margin
786 transition. *Tectonophysics* 509, 218-237.
- 787 Aragón, E., Pinotti, L., Fernando, D., Castro, A., Rabbia, O., Coniglio, J., Demartis, M.,
788 Hernando, I., Cavarozzi, C.E. and Aguilera, Y.E., 2013. The Farallon-Aluk ridge
789 collision with South America: Implications for the geochemical changes of slab window
790 magmas from fore-to back-arc. *Geoscience Frontiers* 4, 377-388.
- 791 Ardolino, A., Busteros, A., Fauqué, L., Franchi, M., Lema, H., 1998. Estratigrafía del cuaternario
792 del litoral patagonico entre Cabo Aristizabal y Bahía Camarones, Provincia del Chubut,
793 Argentina. *Actas X Congreso Latinoamericano de Geología y VI Congreso Nacional de*
794 *Geología Económica* 1, 107–113.
- 795 Balgord, E.A., 2017, Triassic to Neogene evolution of the south-central Andean arc determined
796 by detrital zircon U-Pb and Hf analysis of Neuquén Basin strata, central Argentina
797 (34°S–40°S). *Lithosphere*, 9, 453-462.
- 798 Balgord, E.A., and Carrapa, B., 2016. Basin evolution of Upper Cretaceous–Lower Cenozoic
799 strata in the Malargüe fold-and-thrust belt: northern Neuquén Basin, Argentina. *Basin*
800 *Research*, 28, 183–206.

- 801 Bechis, F., Encinas, A., Concheyro, A., Litvak, V.D., Aguirre-Urreta, B., Ramos, V.A., 2014.
802 New age constraints for the Cenozoic marine transgressions of northwestern Patagonia,
803 Argentina (41°-43°S): Paleogeographic and tectonic implications. *J. S. Am. Earth Sci.* 52,
804 72-93.
- 805 Biddle, K., Uliana, M., Jr., Mitchum, R., Fitzgerald, M. and Wright, R., 1986. The stratigraphic
806 and structural evolution of central and eastern Magallanes Basin, Southern America. *in*
807 *Foreland Basins* (eds P. Allen and P. Homewood), *Int. Assoc. Sedimentol. Spec. Publ.*, 8,
808 41–61.
- 809 Bilmes, A., D'Elia, L., Franzese, J.R., Veiga, G.D., Hernández, M., 2013. Miocene block uplift
810 and basin formation in the Patagonian foreland: the Gastre Basin, Argentina.
811 *Tectonophysics* 601, 98-111.
- 812 Bilmes, A., D'Elia, L., Veiga, G.D., Franzese, J.R., 2014. Relleno intermontano en el antepaís
813 fragmentado patagónico: Evolución neógena de la cuenca de gastre. *Rev. la Asoc. Geol.*
814 *Argentina* 71, 311–330.
- 815 Bouvier, A., Vervoort, J.D., Patchett, P.J., 2008. The Lu–Hf and Sm–Nd isotopic composition of
816 CHUR: Constraints from unequilibrated chondrites and implications for the bulk
817 composition of terrestrial planets. *Earth and Planetary Science Letters.* 273, 48-57.
- 818 Bucher, J., López, M., García, M., Bilmes, A., Elia, L.D., Funes, D., 2018. Estructura y
819 estratigrafía de un bajo neógeno del antepaís norpatagónico : el depocentro Paso del Sapo
820 , provincia de Chubut 75, 312–324.
- 821 Cande, S.C., Leslie, R.B., 1986. Late Cenozoic tectonics of the Southern Chile trench. *J.*
822 *Geophys. Res.* 91, 471–496.
- 823 Castro, A., Moreno-Ventas, I., Fernández, C., Vujovich, G., Gallastegui, G., Heredia, N.,
824 Martino, R.D., Becchio, R., Corretgé, L.G., Díaz-Alvarado, J., Such, P., García-Arias, M.,
825 Liu, D.-Y., 2011. Petrology and SHRIMP U-Pb zircon geochronology of Cordilleran
826 granitoids of the Bariloche area, Argentina. *J. S. Am. Earth Sci.* 32, 508-530.
- 827 Cecil, R., Gehrels, G., Patchett, J., Ducea, M., 2011. U-Pb-Hf characterization of the central
828 Coast Mountains batholith: Implications for petrogenesis and crustal architecture.
829 *Lithosphere.* 3, 247–260.
- 830 Cohen, K.M., Harper, D.A.T., Gibbard, P.L. 2018. ICS International Chronostratigraphic Chart
831 2018/08. International Commission on Stratigraphy, IUGS.

- 832
- 833 Cúneo, R., Ramezani, J., Scasso, R., Diego P., Escapa, I., Zavattieri, A.M., Bowring, S.A., 2013.
834 High-precision U–Pb geochronology and a new chronostratigraphy for the Cañadón
835 Asfalto Basin, Chubut, central Patagonia: Implications for terrestrial faunal and floral
836 evolution in Jurassic. *Gondwana Research* 24, 1267-1275.
- 837 Daniels, B. G., Auchter, N. C., Hubbard, S., Romans, B. W., Matthews, W. A., Stright, L., 2017.
838 Timing of deep-water slope-evolution constrained by large-n detrital and volcanic ash
839 zircon geochronology, Cretaceous Magallanes Basin, Chile. *Geol. Soc. Am. Bull.* 130,
840 438-454.
- 841 de Ignacio, C., López, I., Oyarzun, R., Márquez, A., 2001. The northern Patagonia Somuncura
842 plateau basalts: a product of slab-induced, shallow asthenospheric upwelling? *Terra Nova*
843 13, 117–121.
- 844 Dickinson, W.R., Gehrels, G.E., 2009, Use of U-Pb ages of detrital zircons to infer maximum
845 depositional ages of strata: A test against a Colorado Plateau Mesozoic database: *Earth*
846 *and Planetary Science Letters*, v. 288, no. 1-2, p. 115-125.
- 847 Echaurren, A., Folguera, A., Gianni, G., Orts, D., Tassara, A., Encinas, A., Giménez, M.,
848 Valencia, V., 2016. Tectonic evolution of the North Patagonian Andes (41°–44° S)
849 through recognition of syntectonic strata. *Tectonophysics* 677-678, 99-114.
- 850 Echaurren, A., Oliveros, V., Folguera, A., Ibarra, F., Creixell, C., Lucassen, F., 2017. Early
851 Andean tectonomagmatic stages in north Patagonia: insights from field and geochemical
852 data. *J. Geol. Soc. London* 174, 405-421.
- 853 Encinas, A., Perez, F., Nielsen, S.N., Finger, K.L., Valencia, V., Duhart, P., 2014.
854 Geochronologic and paleontologic evidence for a Pacific-Atlantic connection during the
855 late Oligocene-early Miocene in the Patagonian Andes (43-44°S). *J. S. Am. Earth Sci.* 55,
856 1-18.
- 857 Fernández Paz, L., Litvak, V.D., Echaurren, A., Iannelli, S.B., Encinas, A., Folguera, A.,
858 Valencia, V., 2018. Late Eocene volcanism in North Patagonia (42°30'–43°S): Arc
859 resumption after a stage of within-plate magmatism. *J. Geodyn.* 113, 13-31.
- 860 Figari, E.G., 2005. Evolución tectónica de la Cuenca de Cañadón Asfalto (Zona del valle medio
861 del Río Chubut). Ph.D. thesis. Universidad de Buenos Aires.

- 862 Figari, E.G., Scasso, R.A., Cúneo, R.N., Escapa, I., 2015. Estratigrafía y evolución geológica de
863 la Cuenca de Cañadón Asfalto , Provincia del Chubut , Argentina. *Latin American*
864 *Journal of Sedimentology and Basin Analysis*, v. 22.
- 865 Folguera, A., Encinas, A., Alvarez, O., Orts, D., Gianni, G., Echaurren, A., Litvak, V.D.,
866 Navarrete, C., Sellés, D., Tobal, J., Ramos, M., Fennell, L., Fernández, L, Giménez, M.,
867 Martínez, P., Ruiz, F., Iannelli, S., 2018a, Neogene growth of the Patagonian Andes. In:
868 Folguera A. et al. (eds) *The Evolution of the Chilean-Argentinean Andes*. Springer Earth
869 System Sciences. Springer, Cham, pp. 485-511.
- 870 Folguera, A., Encinas, A., Echaurren, A., Gianni, G., Orts, D. Valencia, V., Carrasco, G., 2018b.
871 Constraints on the Neogene growth of the central Patagonian Andes at the latitude of the
872 Chile triple junction (45°-47°S) using U/Pb geochronology in synorogenic strata.
873 *Tectonophysics* 744, 134-154.
- 874 Folguera, A., Iannizzotto, N.F., 2004. The lagos La Plata and Fontana fold-and-thrust belt: long-
875 lived orogenesis at the edge of western Patagonia. *J. S. Am. Earth Sci.* 16, 541-566.
- 876 Folguera, A., Ramos, V.A., 2011. Repeated eastward shifts of arc magmatism in the Southern
877 Andes: a revision to the long-term pattern of Andean uplift and magmatism. *J. S. Am.*
878 *Earth Sci.* 32, 531-546.
- 879 Fosdick, J.C., Romans, B.W., Fildani, A., Bernhardt, A., Calderón, M., Graham, S.A., 2011.
880 Kinematic evolution of the Patagonian retroarc fold-and-thrust belt and Magallanes
881 foreland basin, Chile and Argentina, 51°30'S. *Geol. Soc. Am. Bull.* 123, 1679-1698.
- 882 Franchi, M.R., Page, R., 1980. Los basaltos cretácicos y la evolución magmática del Chubut
883 occidental. *Rev. Asoc. Geol. Argent.* 35, 208–229.
- 884 Franzese, J.R., D'Elia, L., Bilmes, A., Bucher, J., García, M, López, M., Muravchik, M.,
885 Hernández, M., 2018. Evolution of a Patagonian Miocene intermontane basin and its
886 relationship with the Andean foreland: Tectono-stratigraphic evidences from the Catán Lil
887 Basin, Argentina. *J. S. Am. Earth Sci.* 86, 162-175.
- 888 Franzese, J., Spalletti, L., Pérez, I.G., Macdonald, D., 2003. Tectonic and paleoenvironmental
889 evolution of Mesozoic sedimentary basins along the Andean foothills of Argentina (32–
890 54 S). *J. S. Am. Earth Sci.* 16, 81-90.
- 891 García Morabito, E., Ramos, V.A., 2012. Andean evolution of the Aluminé fold and thrust belt,
892 Northern Patagonian Andes (38°30'-40°30'S). *J. S. Am. Earth Sci.* 38, p. 13-30.

- 893 Gehrels, G.E., Valencia, V., Pullen, A., 2006. Detrital zircon geochronology by Laser-Ablation
894 Multicollector ICPMS at the Arizona LaserChron Center. in Loszewski, T., and Huff, W.,
895 eds., *Geochronology: Emerging Opportunities*, Paleontology Society Short Course:
896 *Paleontology Society Papers*. 11, 1–10.
- 897 Gehrels, G.E., Valencia, V., Ruiz, J., 2008. Enhanced precision, accuracy, efficiency, and spatial
898 resolution of U-Pb ages by laser ablation–multicollector–inductively coupled plasma– mass
899 spectrometry. *Geochemistry Geophysics Geosystems*. 9.
- 900 Gehrels, G., Pecha, M., 2014. Detrital zircon U-Pb geochronology and Hf isotope geochemistry
901 of Paleozoic and Triassic passive margin strata of western North America. *Geosphere*. 10,
902 49–65.
- 903 Ghiglione, M.C., Quinteros, J., Yagupsky, D., Bonillo-Martínez, P., Hlebszevtich, J., Ramos,
904 V.A., Vergani, G., Figueroa, D., Quesada, S., Zapata, T., 2010. Structure and tectonic
905 history of the foreland basins of southernmost South America. *J. South Am. Earth Sci.*
906 *29*, 262–277.
- 907 Giacosa, R.E., Heredia, N., 2004. Structure of the North Patagonian thick-skinned fold-and-
908 thrust belt, southern central Andes, Argentina (41°–42°S), *J. S. Am. Earth Sci.* 18, 61-72.
- 909 Giacosa, R.E., Afonso, J.C., Heredia, N., Paredes, J., 2005. Tertiary tectonics of the sub-Andean
910 region of the North Patagonian Andes, southern central Andes of Argentina (41–
911 42°S30'S). *J. S. Am. Earth Sci.* 20, 157-170.
- 912 Gianni, G., Navarrete, C., Orts, D., Tobal, J., Folguera, A., Giménez, M., 2015. Patagonian
913 broken foreland and related synorogenic rifting: the origin of the Chubut Group Basin.
914 *Tectonophysics* 649, 81-99.
- 915 Gianni, G.M., Dávila, F.M., Echaurren, A., Fennel, L., Tobal, J., Navarrete, C., Quezada, P.,
916 Folguera, A., Giménez, M., 2018. A geodynamic model linking Cretaceous orogeny, arc
917 migration, foreland dynamic subsidence and marine ingression in southern South
918 America. *Earth Sci. Rev.* 185, 437-462.
- 919 González Díaz, E.F., 1982. Chronological zonation of granitic plutonism in the Northern
920 Patagonian Andes of Argentina: the migration of intrusive cycles. *Earth-Science*
921 *Reviews*. 18, 365-393.
- 922 Hauser, N., Cabaleri, N.G., Gallego, O.F., Monferran, M.D., Silva Nieto, D., Armella, C.,
923 Matteini, M., Aparicio González, P.A., Pimentel, M.M., Volkheimer, W., Reimold, W.U.,

- 924 2017. U-Pb and Lu-Hf zircon geochronology of the Cañadón Asfalto Basin, Chubut,
925 Argentina: implications for the magmatic evolution in central Patagonia. *J. S. Am. Earth*
926 *Sci.* 78, 190-212.
- 927 Hervé, F., 1994. The southern Andes between 39° and 44° S latitude: The geological signature of
928 a transpressive tectonic regime related to a magmatic arc. *in* Reutter KJ, Scheuber E,
929 Wigger P (eds) *Tectonics of the southern central Andes*. Springer-Verlag, Berlin. 243–
930 248
- 931 Hervé, F.; Calderón, M.; Fanning, C.M.; Pankhurst, R.J.; Fuentes, F.; Rapela, C.W.; Correa, J.;
932 Quezada, P.; Marambio, C. 2016. Devonian magmatism in the accretionary complex of
933 southern Chile. *J. Geol. Soc. London* 173, 587-602.
- 934 Hervé, F.; Calderón, M.; Fanning, C.M.; Pankhurst, R.J.; Godoy, E. 2013. Provenance variations
935 in the Late Paleozoic accretionary complex of central Chile as indicated by detrital
936 zircons. *Gondwana Research*. 23, 112-113.
- 937 Hervé, F., Calderón, M., Fanning, M., Pankhurst, R.J., Rapela, C.W., Quezada, P., 2018. The
938 country rocks of Devonian magmatism in the North Patagonian Massif and Chaitenia.
939 *Andean Geology*. 45, 301-317.
- 940 Horton, B.K., and Fuentes, F., 2016. Sedimentary record of plate coupling and decoupling during
941 growth of the Andes. *Geology*. 44, 647-650.
- 942 Horton, B.K., Fuentes, F., Boll, A., Starck, D., Ramirez, S.G., Stockli, D.F., 2016. Andean
943 stratigraphic record of the transition from backarc extension to orogenic shortening: A
944 case study from the northern Neuquén Basin, Argentina. *J. S. Am. Earth Sci.* 71, 17-40.
- 945 Horton, B.K., Perez, N.D., Fitch, J.D., and Saylor, J.E., 2015. Punctuated shortening and
946 subsidence in the Altiplano plateau of southern Peru: Implications for early Andean
947 mountain building. *Lithosphere*. 7, 117–137.
- 948 Horton, B.K., 2018a. Sedimentary record of Andean mountain building. *Earth Sci. Rev.* 178,
949 279-309, doi:10.1016/j.earscirev.2017.11.025.
- 950 Horton, B.K., 2018b. Tectonic regimes of the central and southern Andes: Responses to
951 variations in plate coupling during subduction. *Tectonics* 37, 402–429,
952 doi:10.1002/2017TC004624.
- 953 Howell, J.A., Schwarz, E., Spalletti, L.A., Veiga, G.D., 2005. The Neuquén Basin: an overview.
954 *Geol. Soc. London, Spec. Publ.* 252, 1–14.

- 955 Iannelli, S.B, Fennell, L.M., Litvak, V.D., Fernández, P.L., Encinas, A., Folguera, A., 2018.
956 Geochemical and tectonic evolution of Late Cretaceous to early Paleocene magmatism
957 along the Southern Central Andes (35-36 S). *J. S. Am. Earth Sci.* 87, 139-156.
- 958 Iannelli, S.B., Litvak, V.D., Fernandez Paz, Folguera, A., Ramos, M.E., Ramos, V.A., 2017.
959 Evolution of Eocene to Oligocene arc-related volcanism in the North Patagonian Andes
960 (39-41°S), prior to the break up of the Farallon plate. *Tectonophysics.* 696-697, 70-87.
- 961 Jordan, T.E, Burns, W.M., Veiga, R., Pángaro, F., Copeland, P., Kelley, S., Mpodozis, 2001.
962 Extension and basin formation in the southern Andes caused by increased convergence
963 rate: A mid-Cenozoic trigger for the Andes. *Tectonics.* 20, 308-234.
- 964 Kay, S.M., Ardolino, A.A., Gorring, M.L., Ramos, V.A., 2007. The Somuncura large igneous
965 province in Patagonia: Interaction of a transient mantle thermal anomaly with a
966 subducting slab. *J. Petrol.* 48, 43–77.
- 967 Lizuáin A. and Viera R., 2010. Descripción geológica de la Hoja 4372-I y II, Esquel, Provincia
968 de Chubut. Servicio Geológico Minero Argentino, Instituto de Geología y Recursos
969 Minerales, Boletín. 369, 1–92.
- 970 Ludwig, K.R., 2003. User's Manual for Isoplot 3.60: A Geochronological Toolkit for Microsoft
971 Excel: Berkeley Geochronology Center Special Publication, v. 4, p. 77.
- 972 Ludwig, K.R., 2008. Isoplot/Ex 3.70: A geochronological toolkit for Microsoft Excel. Berkley
973 Geochronologic Center Special Publication. 4, 1-77.
- 974 López, Manuel & García, Micaela & Bucher, Joaquin & S. Funes, Daniela & D'Elia, Leandro &
975 Bilmes, Andrés & Naipauer, Maximiliano & M. Sato, Ana & A. Valencia, Victor &
976 Franzese, Juan, 2019. Structural evolution of The Collón Cura basin: Tectonic implications
977 for the north Patagonian Broken Foreland. *Journal of South American Earth Sciences.*
- 978 Marveggio, N., Llorens, M., 2013. Nueva edad de la base del Grupo Chubut en la mena uranífera
979 Cerro Solo, provincia del Chubut. *Rev. Asoc. Geol. Argent.* 70, 318-326.
- 980 Mazzoni, M., Kawashita K., Harrison, S., Aragón, E., 1991, Edades radiométricas eocenas, Borde
981 occidental del Macizo Norpatagónico. *Revista de la Asociación Geológica Argentina*, 46,
982 150–158.
- 983 Muñoz, J., Araneda, M. and McDonough, M., 1998. Geofísica Regional. In SERNAGEOMIN,
984 1998. Estudio Geológico-Económico de la X Región Norte (Inédito), Servicio Nacional
985 de Geología y Minería, Informe Registrado IR-15-98, v.6

- 986 Muñoz, J., Troncoso, R., Dunhart, P., Crignola, P., Farmer, L., Stern, C.R., 2000. The relation of
987 the mid-Tertiary coastal magmatic belt in south-central Chile to the late Oligocene
988 increase in convergence rate. *Rev. Asoc. Geol. Argent.* 27, 1-23.
- 989 Navarro, E.L., Astini, R.A., Belousova, E., Guler, M.V., Gehrels, G., 2015. Detrital zircon
990 geochronology and provenance of the Chubut Group in the northeast of Patagonia,
991 Argentina. *J. S. Am. Earth Sci.* 63, 149-161.
- 992 Navarrete, C., Gianni, G., Echaurren, A., Kingler, F.L., Folguera, A., 2016. Episodic Jurassic to
993 Lower Cretaceous intraplate compression in Central Patagonia during Gondwana
994 breakup. *J. Geodyn.* 102, 185–201, doi:10.1016/j.jog.2016.10.001.
- 995 Orts, D., Folguera, A., Encinas, A., Ramos, M., Tobal, J., Ramos, V.A., 2012. Tectonic
996 development of the North Patagonian Andes and their related Miocene foreland basin
997 (41°30'-43°S). *Tectonics* 31, TC3012, doi:10.1029/2011TC003084.
- 998 Orts, D.L., Folguera, A., Giménez, M., Ruiz, F., Rojas Vera, E.A., Klinger, F.L., 2015. Cenozoic
999 building and deformational processes in the North Patagonian Andes. *J. Geodyn.* 86, 26-41.
- 1000 Pankhurst, R. J., Hervé, F., Rapela, C.W., 1994. Sm-Nd evidence for the Grenvillian provenance
1001 of the metasedimentary basement of Southern Chile and West Antarctica. In 7° Congreso
1002 Geológico Chileno, Concepción, Actas, 2, 1414-1418.
- 1003 Pankhurst R.J., Rapela, C.R., 1995. Production of Jurassic rhyolite by anatexis of the lower crust
1004 of Patagonia. *Earth and Planetary Science Letters* 134, 23-36.
- 1005 Pankhurst, R.J., Rapela, C.W., Fanning, C.M., Márquez, M., 2006. Gondwanide continental
1006 collision and the origin of Patagonia. *Earth Sci. Rev.* 76, 235-257.
- 1007 Pankhurst, R.J., Riley, T.R., Fanning, C.M., Kelley, S.P., 2000. Episodic silicic volcanism in
1008 Patagonia and Antarctic peninsula: chronology of the magmatism associated with the
1009 break-up of Gondwana. *J. Petrology* 41, 605-625.
- 1010 Pankhurst, R.J., Weaver, S.D., Hervé, F., Larrondo, P., 1999. Mesozoic-Cenozoic evolution of
1011 the North Patagonian Batholith in Aysén, southern Chile. *J. Geol. Soc. London* 156, 673-
1012 694.
- 1013 Pepper, M., Gehrels, G., Pullen, A., Ibanez-Mejia, M., Ward, K.M., Kapp, P., 2016. Magmatic
1014 history and crustal genesis of western South America: Constraints from U-Pb ages and Hf
1015 isotopes of detrital zircons in modern rivers. *Geosphere* 12, 1532-1555.
- 1016 Ramos, V.A., 2008. Patagonia: A paleozoic continent adrift? *J. S. Am. Earth Sci.* 26, 235–251.

- 1017 Ramos, V.A., 2009. Anatomy and global context of the Andes: Main geologic features and the
1018 orogenic cycle. In: Kay, S.M., Ramos, V.A., Dickinson, W.R., eds., Backbone of the
1019 Americas: Shallow Subduction, Plateau Uplift, and Ridge and Terrane Collision: Geol.
1020 Soc. Am. Mem. 204, 31–65
- 1021 Ramos, M.E., Tobal, J.E., Sagripanti, L., Folguera, A., Orts, D.L., Giménez, M., Ramos, V.A.,
1022 2015. The North Patagonian orogenic front and related foreland evolution during the
1023 Miocene, analyzed from synorogenic sedimentation and U/Pb dating (~42°S). *J. S. Am.*
1024 *Earth Sci.* 64, 467-485.
- 1025 Rapela, C.W., Pankhurst, R.J., 1992. The granite of northern Patagonia and the Gastre Fault
1026 System in relation to the break-up of Gondwana. In Storey, B.C., Alabaster, T. and
1027 Pankhurst, R.J. (eds) *Magmatism and the Causes of Continental Break-up*. Geol. Soc.
1028 London, Spec. Publ. 68, 209-220.
- 1029 Rapela, C.W., Pankhurst, R.J., Fanning, C.M., and Hervé, F., 2005. Pacific subduction coeval
1030 with the Karoo mantle plume: the Early Jurassic Subcordilleran belt of northwestern
1031 Patagonia. *in* Vaughan, A.P.M., Leat, P.T., and Pankhurst, R.J. (eds). *Terrane Processes at*
1032 *the Margins of Gondwana*. Geological Society, London, Special Publications, v. 246, p.
1033 217-239.
- 1034 Rapela, C.W., Spalletti, L. A., Merodio, J. C., Aragón, E., 1988. Temporal evolution and spatial
1035 variation of early Tertiary volcanism in the Patagonian Andes (40°S-42°30'S). *J. S. Am.*
1036 *Earth Sci.* 1, 75-88.
- 1037 Rolando, A., Hartmann, L., Orestes, J., Fernández, R., Etcheverry, R., Schalamuk, I., and
1038 McNaughton, N., 2002. SHRIMP zircon U-Pb evidence for extended Mesozoic magmatism
1039 in the Patagonian Batholith and assimilation of Archean crustal components. *Journal of*
1040 *South American Earth Sciences*, 15: 267-283.
- 1041 Rolando, A. P., Hartmann, L. A., Santos, J. O. S., Fernandez, R. R., Etcheverry, R. O.,
1042 Schalamuk, I. A., McNaughton, N. J., 2004. SHRIMP zircon U-Pb evidence for extended
1043 Mesozoic magmatism in the Patagonian Batholith and assimilation of Archean crustal
1044 components. *Journal of South American Earth Sciences*, 15, 267–283.
- 1045 Romans, B.W., Hubbard, S.M., Covault, J.A., Fosdick, J.C. & Graham, S.A., 2011. Evolution of
1046 deep-water stratigraphic architecture, Magallanes Basin, Chile. *Mar. Pet. Geol.*, 28, 612–
1047 628.

- 1048 Savignano, E., Mazzoli, S., Arce, M., Franchini, M., Gautheron, C., Paolini, M., Zattin, M.,
1049 2016. (Un)Coupled thrust belt-foreland deformation in the northern Patagonian Andes:
1050 New insights from the Esquel-Gastre sector (41°30'–43°S). *Tectonics* 35, 2636-2656.
- 1051 Scasso, R.A., Alberhan, M., Ruiz, L., Weidemeyer, S., Medina, F.A., Kiessling, W., 2012.
1052 Integrated bio- and lithofacies analysis of coarse-grained, tide-dominated deltaic
1053 environments across the Cretaceous/Paleogene boundary in Patagonia, Argentina.
1054 *Cretaceous Research* 36, 37-57.
- 1055 Schwartz, T.M., Fosdick, J.C., Graham, S.A., 2017. Using detrital zircon U-Pb ages to calculate
1056 Late Cretaceous sedimentation rates in the Magallanes-Austral basin, Patagonia. *Basin*
1057 *Res.*, 29, 725-746.
- 1058 Spalletti, L.A., 1996. Estuarine and shallow-marine sedimentation in the Upper Cretaceous
1059 Lower Tertiary west-central Patagonian Basin (Argentina). In: de Batist, M., Jacobs, P.
1060 (Eds.), *Geology of Siliciclastic Shelf Seas*. Geol. Soc. London, Spec. Publ. 117, 81-93.
- 1061 Spalletti, L.A., and Dalla Salda, L.H., 1996. A pull apart volcanic related Tertiary basin, an
1062 example from the Patagonian Andes. *Journal of South American Earth Sciences*, v. 9., p.
1063 197-206.
- 1064 Suárez, M., de la Cruz, R., 2001. Jurassic to Miocene K–Ar dates from eastern central
1065 Patagonian Cordillera plutons, Chile (45°–48° S). *Geol. Mag.* 183, 53-66.
- 1066 Suárez, M., De La Cruz, R., Bell, M., Demant, A., 2010. Cretaceous slab segmentation in
1067 southwestern Gondwana. *Geol. Mag.* 147, 193-205.
- 1068 Suárez, M., De la Cruz, R., Aguirre-Urreta, B., Fanning, M., 2009a. Relationship between
1069 volcanism and marine sedimentation in northern Austral (Aisén) Basin, central Patagonia:
1070 Stratigraphic, U–Pb SHRIMP and paleontologic evidence. *Journal of South American*
1071 *Earth Sciences*, 27, 309-325.
- 1072 Suárez, M., Marquez, M., De La Cruz, R., Fanning, M., 2009b. Aptian-Albian subaerial volcanic
1073 rocks in central Patagonia: Divisadero and Chubut Groups. XII Congreso Geológico
1074 Chileno, Santiago.
- 1075 Suárez, M., Márquez, M., De La Cruz, R., Navarrete, C., Fanning, M., 2014. Cenomanian-? early
1076 Turonian minimum age of the Chubut Group, Argentina: SHRIMP U-Pb geochronology.
1077 *J. S. Am. Earth Sci.* 50, 67-74.

- 1078 Thomson, S.N., 2002. Late Cenozoic geomorphic and tectonic evolution of the Patagonian
1079 Andes between latitudes 42°S and 46°S: An appraisal based on fission-track results from
1080 the transpressional intra-arc Liquiñe-Ofqui fault zone. *Geol. Soc. Am. Bull.* 114, 1159-
1081 1173.
- 1082 Thomson, S.N., Hervé, F., Stöckhert, B., 2001. Mesozoic-Cenozoic denudation history of the
1083 Patagonian Andes (southern Chile) and its correlation to different subduction processes.
1084 *Tectonics* 20, 693-711.
- 1085 Uliana, M.A., Biddle, K.T., Cerdan, J., 1989. Mesozoic extension and the formation of Argentine
1086 sedimentary basins. *American Association of Petroleum Geologists Memoir* 46, 599–614.
- 1087 Vervoort, J. D., Blichert-Toft, J., 1999. Evolution of the depleted mantle: Hf isotope evidence
1088 from juvenile rocks through time. *Geochimica et Cosmochimica Acta*/ 63, 533-556.
- 1089 Vervoort, J. D., Patchett, P. J., 1996. Behavior of hafnium and neodymium isotopes in the crust:
1090 constraints from Precambrian crustally derived granites. *Geochimica et Cosmochimica*
1091 *Acta.* 60, 3717-3733.
- 1092 Vervoort, J. D., Blichert-Toft, J., 1999. Evolution of the depleted mantle: Hf isotope evidence
1093 from juvenile rocks through time. *Geochimica et Cosmochimica Acta.* 63, 533-556.
- 1094 Wilf, P., Singer, B.S., Zamalao, M., Johnson, K.R., Cúneo, N.R., 2010. Early Eocene 40Ar/39Ar
1095 age for the Pampa de Jones plant, frog, and insect biota (Huitrera Formation, Neuquén
1096 Province, Patagonia, Argentina). *AMEGHINIANA Rev. Asoc. Paleontol. Argent.* 47, 207-
1097 216.
- 1098 Zaffarana, C., Lagorio, S., Orts, D., Busteros, A., Nieto, D.S., Giacosa, R., Gonzalez, V.R.,
1099 Bolthausen, B., Negre, C.P., Somoza, R., Haller, M., 2018. First geochemical and
1100 geochronological characterization of Late Cretaceous mesosilicic magmatism in Gastre,
1101 Northern Patagonia, and its tectonic relation to other coeval volcanic rocks in the region.
1102 *Geol. Mag.*, doi:10.1017/S0016756818000432
- 1103 Zaffarana, C.B., Lagorio S.L., Somoza, R., 2012a. Paleomagnetism and geochemistry from the
1104 Upper Cretaceous Tres Picos Prieto locality (43°S), Patagonian Plateau Basalts. *Andean*
1105 *Geology.* 39, 53-66.
- 1106 Zaffarana, C.B., Somoza, R., 2012b. Palaeomagnetism and 40Ar/39Ar dating from Lower
1107 Jurassic rocks in Gastre, central Patagonia: further data to explore tectonomagmatic

- 1108 events associated with the break-up of Gondwana. *Journal of the Geological Society of*
1109 *London*. 169, 371-379.
- 1110 Zaffarana, C.B., Somoza, R., López de Luchi, M., 2014. The Late Triassic Central Patagonian
1111 Batholith: Magma hybridization, $^{40}\text{Ar}/^{39}\text{Ar}$ ages and thermobarometry. *Journal of South*
1112 *American Earth Sciences* 55, 94-122.
- 1113

1114 **TABLE CAPTIONS**

1115

1116 **Table 1.** Summary table listing sample location, formation, stratigraphic position and analyses.

1117

1118 **Table 2.** Summary table listing the maximum depositional age (MDA) on the basis of the
1119 youngest age peak, youngest single grain, or youngest 2+ grains that overlap at 2σ .

1120

1121 **FIGURE CAPTIONS**

1122

1123 **Figure 1.** Simplified regional map of southern South America showing sedimentary basins
1124 (Neuquén Basin, Patagonian broken foreland, and Magallanes-Austral Basin), basement
1125 provinces (North Patagonian Massif and Deseado Massif), modern tectonic plate boundaries
1126 (Nazca, Antarctic, South American, and Scotia plates), and key orogenic elements (from west to
1127 east, the Chile Rise, Chile trench, Coastal Range, Central Valley, Liquiñe-Ofqui fault zone
1128 (LOFZ), North Patagonian Andes, deformation front of the North Patagonian fold-thrust belt
1129 (teeth), and North Patagonian Precordillera).

1130

1131 **Figure 2.** Geologic map of northern Patagonia depicting major structures, sample and growth
1132 strata localities (after Ardolino et al., 1998; and Lizuaín, 1995). Corresponding chart shows the
1133 names of geologic units of variable age: Paleozoic (Pz), Triassic (Tr), Jurassic (J), Cretaceous
1134 (K), Paleogene (Pg), and Neogene (Ng).

1135

1136 **Figure 3.** Cretaceous-Paleogene-Neogene stratigraphic chart for the Patagonian broken foreland
1137 showing stratigraphic units and sampled stratigraphic level, growth strata intervals, hiatuses,
1138 unconformities, and maximum depositional ages.

1139 Timescale after Cohen et al (2018).

1140

1141 **Figure 4.** (A) Phanerozoic stratigraphic chart for western and eastern sediment source regions in
1142 northern Patagonia at ~ 40 – 44°S showing the name, age, and lithology of various geologic units,
1143 including published isotopic ages. (B) Plots of the composite age distributions for the western
1144 source region (pre-Andean basement) and eastern source region (North Patagonian Massif)

1145 showing probability density plots (shaded colors) and age histograms (thin rectangles), with bold
1146 numerals identifying age peaks (in Ma).

1147

1148 **Figure 5.**

1149 Plots showing the youngest detrital zircon U-Pb age populations for individual samples. WMA =
1150 weighted mean age, MSWD = mean square weighted deviation.

1151

1152 **Figure 6.** Detrital zircon U-Pb age data for 17 samples of Cretaceous-Cenozoic stratigraphic
1153 units and a composite age distribution (base), shown as probability density plots (thick curves)
1154 and age histograms (thin rectangles), arranged in approximate stratigraphic order. For each age
1155 distribution, bold numerals identify age peaks (in Ma) and italicized values identify maximum
1156 depositional ages (MDAs) that may approximate true depositional ages. Shaded color rectangles
1157 identify diagnostic age populations.

1158

1159 **Figure 7.** (A) Hf evolution diagram and (B) corresponding detrital zircon U-Pb composite age
1160 data (below) for 200–0 Ma record in the North Patagonian broken foreland. Shaded gray arrows
1161 show running mean of the isotopic data and identify general temporal trends in Hf isotope
1162 values. CHUR = chondritic bulk reservoir. Average crustal evolution = trajectory with present-
1163 day $^{176}\text{Lu}/^{177}\text{Hf} = 0.0115$ (Vervoort and Patchett, 1996; Vervoort et al., 1999).

1164

1165 **Figure 8.** Field photographs and line drawings of growth stratal packages in (A) the middle
1166 Miocene upper levels of the Ñirihuau Formation exposed in the Esquel Range of the North
1167 Patagonian foothills (after Echaurren et al., 2016) and (B) the late Miocene upper levels of the
1168 Collón Curá Formation in the broken foreland region adjacent to the Cordón del Maitén (after
1169 Ramos et al., 2015). Stratal dip values and maximum depositional ages (MDAs) for sandstone
1170 samples with young zircon U-Pb age populations (Fig. 5) are shown for pre-growth strata (light
1171 shading) and growth strata (dark shading).

1172

1173 **Figure 9.** Time-space plot showing the distribution of Middle Jurassic to Neogene (170–0 Ma)
1174 isotopic ages representing Andean arc magmatism at $\sim 40\text{--}46^\circ\text{S}$. Detrital zircon U-Pb composite
1175 age data (below) for 200–0 Ma record in the Patagonian broken foreland. Arrows denote

1176 interpreted phases of arc advance (Campanian-Maastrichtian), arc cessation (Paleocene-Eocene),
1177 and arc retreat (middle-late Miocene).

1178

1179 **Figure 10.** Time-space plot showing the Mesozoic-Cenozoic history of northern Patagonia (~40-
1180 46°S), including arc magmatic trends, igneous affinities, deformational modes, sedimentary
1181 basin development, fault and paleoflow orientations, periods of sedimentation and non-
1182 deposition (hiatuses), and marine incursions.

1183

Broken foreland segment	Sample	Group	Formation	Position	Latitude	Longitude	Reference	Analyses
Eastern	17TQT03	Chubut Group	Los Adobes	uppermost	42°57'25.02"S	69°13'15.07"W	this study	DZ U-Pb
	SJS		Cerro Barcino	unknown			Navarro et al, 2015	
	TS2		Cerro Barcino	unknown			Navarro et al, 2015	
Central	17PDS04		Paso del Sapo	base	42°40'54.12"S	69°45'4.57"W	this study	DZ U-Pb/Lu-Hf
	17TQT01			base	42°55'7.00"S	69°15'2.22"W	this study	DZ U-Pb/Lu-Hf
	17PDS19			top	42°40'9.12"S	69°51'22.73"W	this study	DZ U-Pb
	PS-01				unknown		Echaurren et al, 2017	
	17PDS20		Lefipán	base	42°40'9.12"S	69°51'22.73"W	this study	DZ U-Pb
Western	17ESQ01		Ñirihuau	lower	42°51'21.20"S	71°20'11.98"W	this study	DZ U-Pb/Lu-Hf
	17CUS02			lower	42°4'16.61"S	71°1'32.70"W	this study	DZ U-Pb/Lu-Hf
	17CUS03			lower	42°4'16.61"S	71°1'32.70"W	this study	DZ U-Pb
	17ESQ02			upper	42°59'6.29"S	71°29'21.77"W	this study	DZ U-Pb
	17ESQ03			upper	42°59'6.29"S	71°29'21.77"W	this study	DZ U-Pb
	17CUS04		Collón Curá	upper	42° 5'51.14"S	70°55'11.28"W	this study	DZ U-Pb
	17CUS05			upper	42° 5'51.14"S	70°55'11.28"W	this study	DZ U-Pb
	17TEC01			lower	43°23'32.89"S	70°44'27.85"W	this study	DZ U-Pb
	17PDS02		La Pava	lower	42°40'59.27"S	69°39'41.40"W	this study	DZ U-Pb

Table 1. Summary table listing sample location, formation, stratigraphic position and analyses.

Growth structure	Growth strata position	Sample	Formation	Youngest age peak (n=)	Youngest single grain Ma \pm 2 σ	Youngest 2+ grains Ma \pm 2 σ	Preferred MDA Ma \pm 2 σ	Stratigraphic age	
Cordón del Maitén	lower growth	17CUS05	Collón Curá	16 (13)	9.3 \pm 0.3			Tortonian	
		pre-growth	17CUS04	Collón Curá	14 (13)	9.9 \pm 0.4	10.1 \pm 0.2 (0.51)	10.1 \pm 0.2 (3)	Tortonian
			17PDS02	Collón Curá	18 (14)	14.5 \pm 0.6	14.7 \pm 0.2 (0.77)	14.6 \pm 0.4 (2)	Langhian
			17TEC01	Collón Curá	15 (9)	14.5 \pm 0.5		14.7 \pm 0.2 (5)	Langhian
Esquel Range	lower growth	17ESQ03	Ñirihuau		12.4 \pm 0.5		12.5 \pm 0.3 (2)	Langhian	
	pre-growth	17ESQ02	Ñirihuau	13 (10)	12.9 \pm 0.4	13.1 \pm 0.2 (0.59)	13.1 \pm 0.2 (5)	Serravallian	
	pre-growth	17ESQ01	Ñirihuau	17 (63)	16.3 \pm 0.5	16.9 \pm 0.1 (0.96)	16.9 \pm 0.1 (33)	Burdigalian	
Cordón del Maitén	lower growth	17CUS03	Ñirihuau	22 (5)	21.5 \pm 1.0	22.2 \pm 0.3 (1.03)	22.2 \pm 0.3 (7)	Burdigalian	
	lower growth	17CUS02	Ñirihuau	41 (5)	36.4 \pm 1.5	37.6 \pm 2.2 (2.9)			
Taquetrén Range	lower growth	17PDS20	Lefipán	82 (2)	81.4 \pm 1.8				
		17PDS19	Paso del Sapo	83 (10)	71.9 \pm 1.8			Mastrichtian	
		PS-01	Paso del Sapo	82 (6)	81.1 \pm 3.0			Mastrichtian	
		17TQT01	Paso del Sapo	87 (5)	70.9 \pm 1.4			Mastrichtian	
		17PDS04	Paso del Sapo	72 (3)	71 \pm 2.4	73.4 \pm 4.5 (3.1)	73.4 \pm 4.5 (3)	Mastrichtian	
		T2S	Cerro Barcino	109 (7)	102 \pm 6.8	112 \pm 11 (1.8)	112 \pm 11 (5)	Albian	
		SJS	Cerro Barcino	109 (7)	103 \pm 2	107 \pm 4.3 (1.8)	107 \pm 4.3 (4)	Albian	
		17TQT03	Los Adobes	182 (24)	106.9 \pm 2.2			Albian	

Table 2. Summary table listing the maximum depositional age (MDA) on the basis of the youngest age peak, youngest single grain, or youngest 2+ grains that overlap at 2 σ .

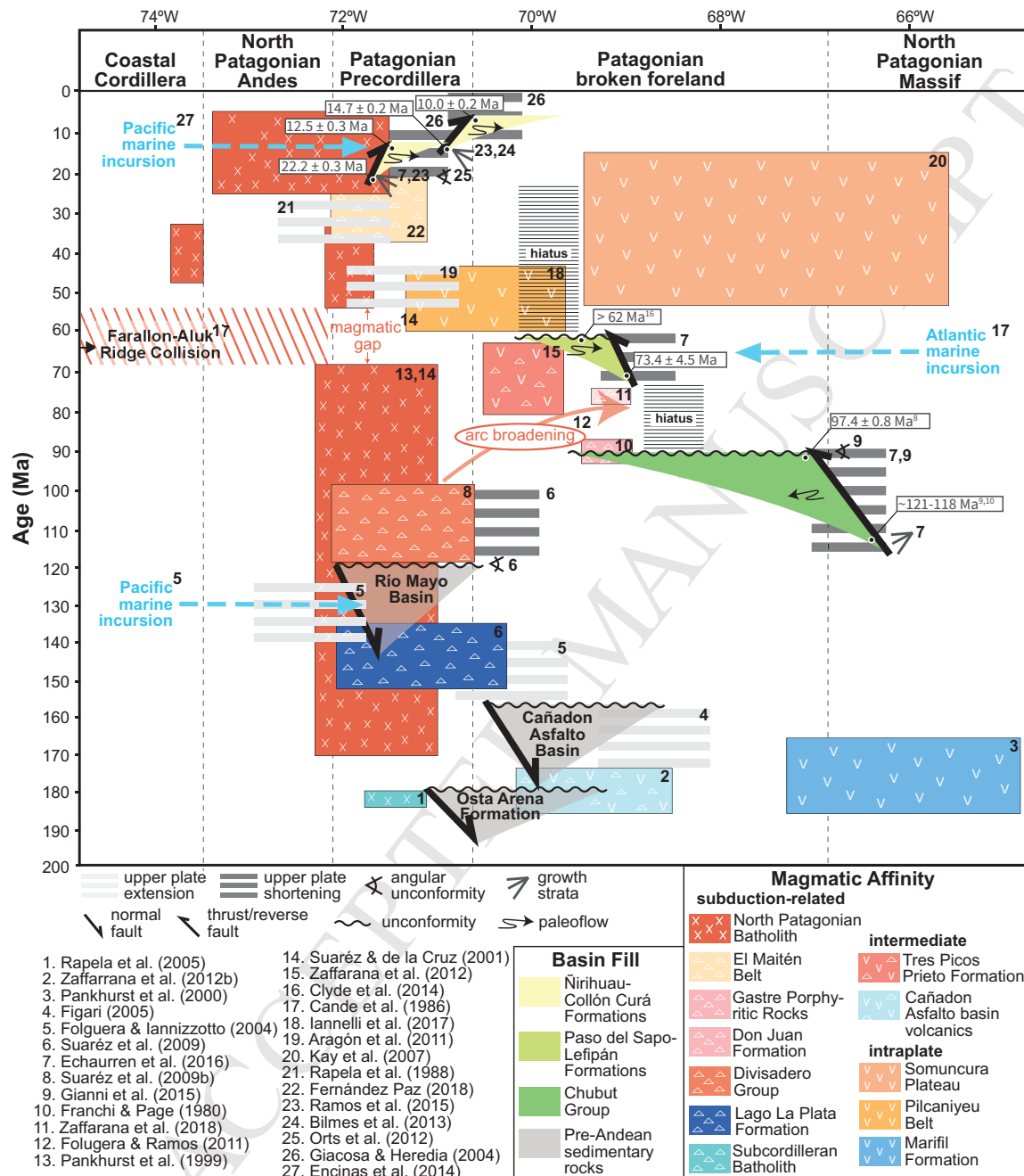


Figure 10. Time-space plot showing the Mesozoic-Cenozoic history of northern Patagonia (~40-46°S), including arc magmatic trends, igneous affinities, deformational modes, sedimentary basin development, fault and paleoflow orientations, periods of sedimentation and non-deposition (hiatuses), and marine incursions.

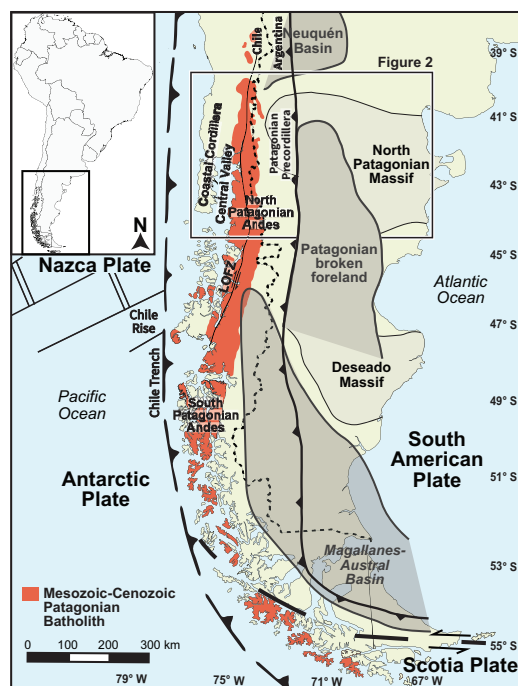
Butler et al., Figure 1
1 column width

Figure 1. Simplified regional map of southern South America showing sedimentary basins (Neuquén Basin, North Patagonia broken foreland, and Austral-Magallanes Basin), basement provinces (Patagonian Massif and Deseado Massif), modern tectonic plate boundaries (Nazca, Antarctic, South American, and Scotia plates), and key orogenic elements (from west to east, the Chile Rise, Chile trench, Coastal Cordillera, Central Valley, Liqueñe-Ofqui fault zone (LOFZ), North Patagonian Andes, deformation front of the North Patagonian fold-thrust belt (teeth), and Patagonian Precordillera).

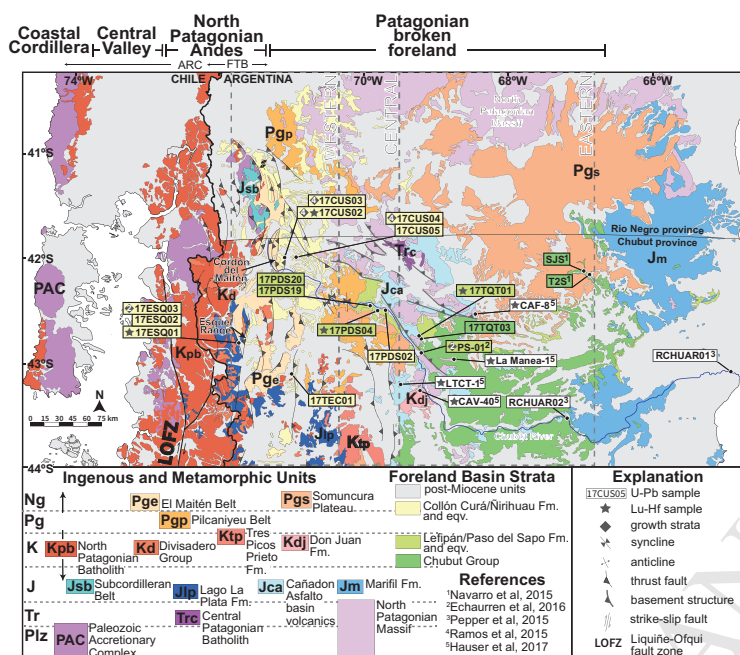
Butler et al., Figure 2
2 column width

Figure 2. Geologic map of northern Patagonia depicting major structures, sample and growth strata localities (after Ardolino et al., 1998; and Lizuain, 1995). Corresponding chart shows the names of geologic units of variable age: Paleozoic (Pz), Triassic (Tr), Jurassic (J), Cretaceous (K), Paleogene (Pg), and Neogene (Ng). FTB = fold-thrust belt (Patagonian Precordillera), Arc = Andean magmatic arc.

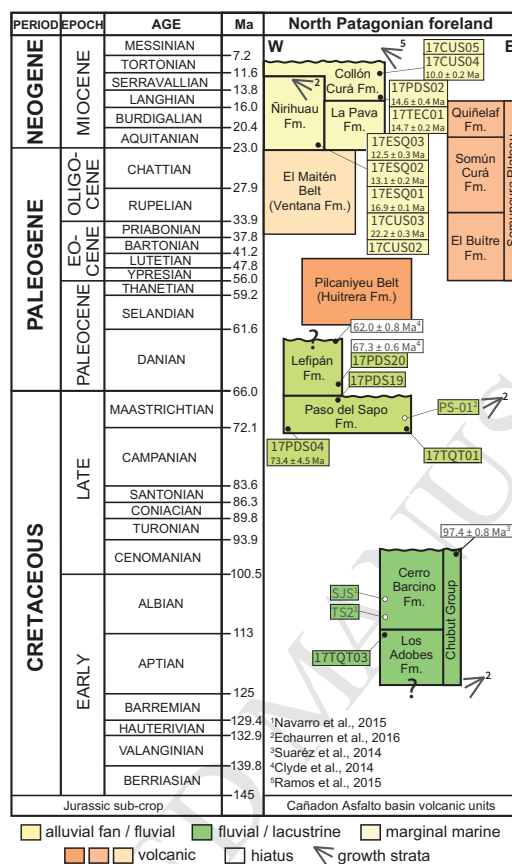


Figure 3. Cretaceous-Paleogene-Neogene stratigraphic chart for the Patagonian broken foreland showing stratigraphic units and sampled stratigraphic level, growth strata intervals, hiatuses, unconformities, and maximum depositional ages. Timescale after Cohen et al (2018).

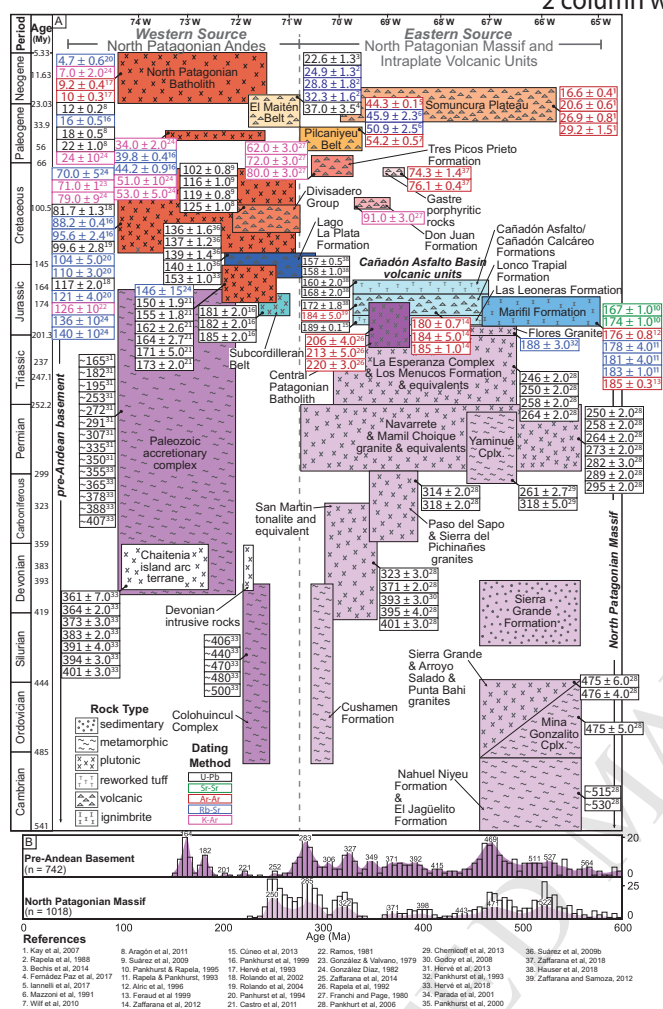
Butler et al., Figure 4
2 column width

Figure 4. (A) Phanerozoic stratigraphic chart for western and eastern sediment source regions in northern Patagonia at ~ 40 – 44° S showing the name, age, and lithology of various geologic units, including published isotopic ages. (B) Plots of the composite age distributions for the western source region (pre-Andean basement) and eastern source region (North Patagonian Massif) showing probability density plots (shaded colors) and age histograms (thin rectangles), with bold numerals identifying age peaks (in Ma).

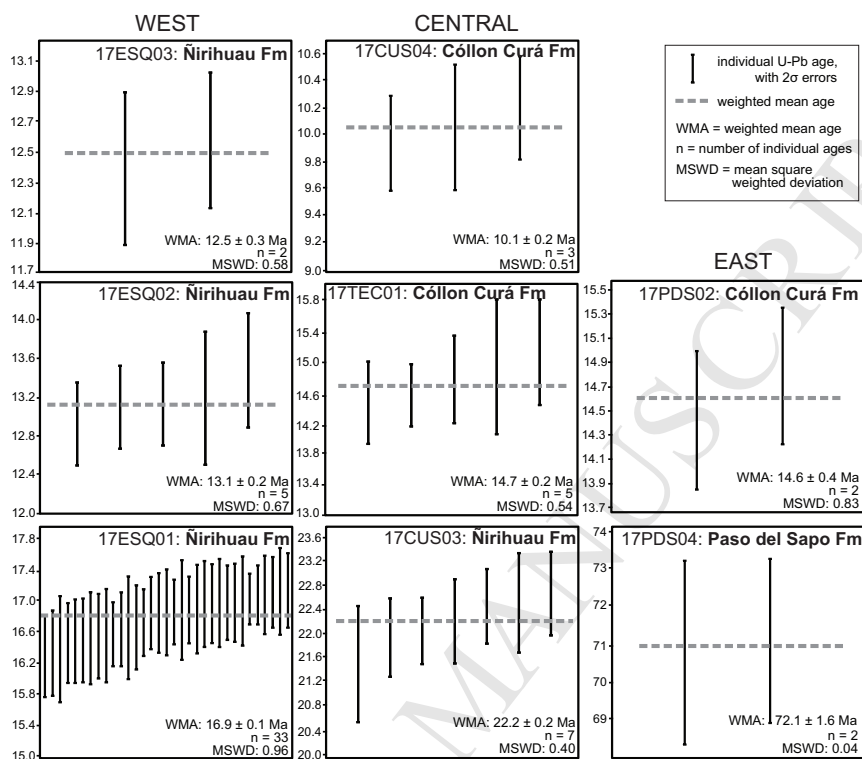
Butler et al., Figure 5
2 column width

Figure 5. Plots showing the youngest detrital zircon U-Pb age populations for individual samples. WMA = weighted mean age, MSWD = mean square weighted deviation.

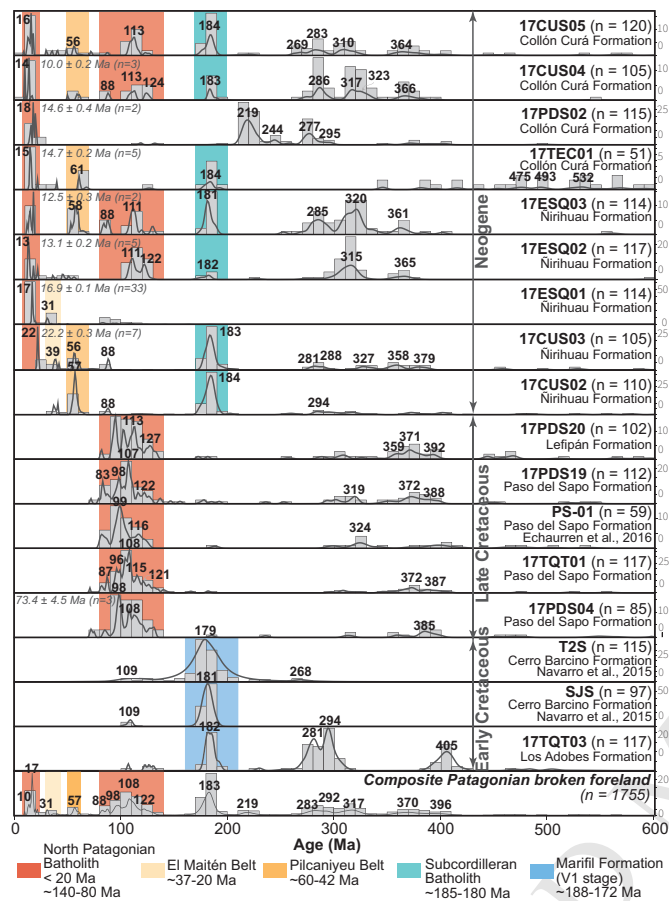
Butler et al., Figure 6
2 column width

Figure 6. Detrital zircon U-Pb age data for 17 samples of Cretaceous-Cenozoic stratigraphic units and a composite age distribution (base), shown as probability density plots (thick curves) and age histograms (thin rectangles), arranged in approximate stratigraphic order. For each age distribution, bold numerals identify age peaks (in Ma) and italicized values identify maximum depositional ages (MDAs) that may approximate true depositional ages. Shaded color rectangles identify diagnostic age populations.

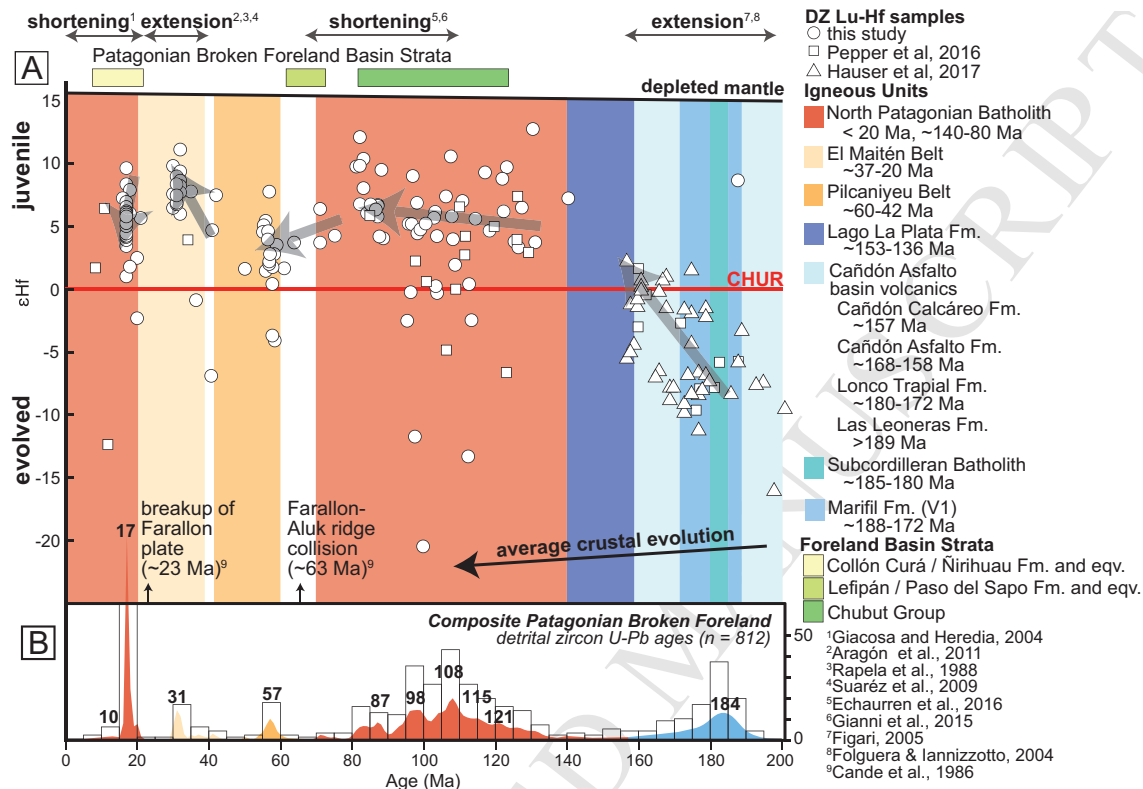
Butler et al., Figure 7
2 column width

Figure 7. (A) Hf evolution diagram and (B) corresponding detrital zircon U-Pb composite age data (below) for 200–0 Ma record in the North Patagonian broken foreland. Shaded gray arrows show running mean of the isotopic data and identify general temporal trends in Hf isotope values. CHUR = chondritic bulk reservoir. Average crustal evolution = trajectory with present-day $^{176}\text{Lu}/^{177}\text{Hf} = 0.0115$ (Vervoort and Patchett, 1996; Vervoort et al., 1999). Measured $^{176}\text{Hf}/^{177}\text{Hf}$ uncertainties are ~1 epsilon unit (1ϵ).

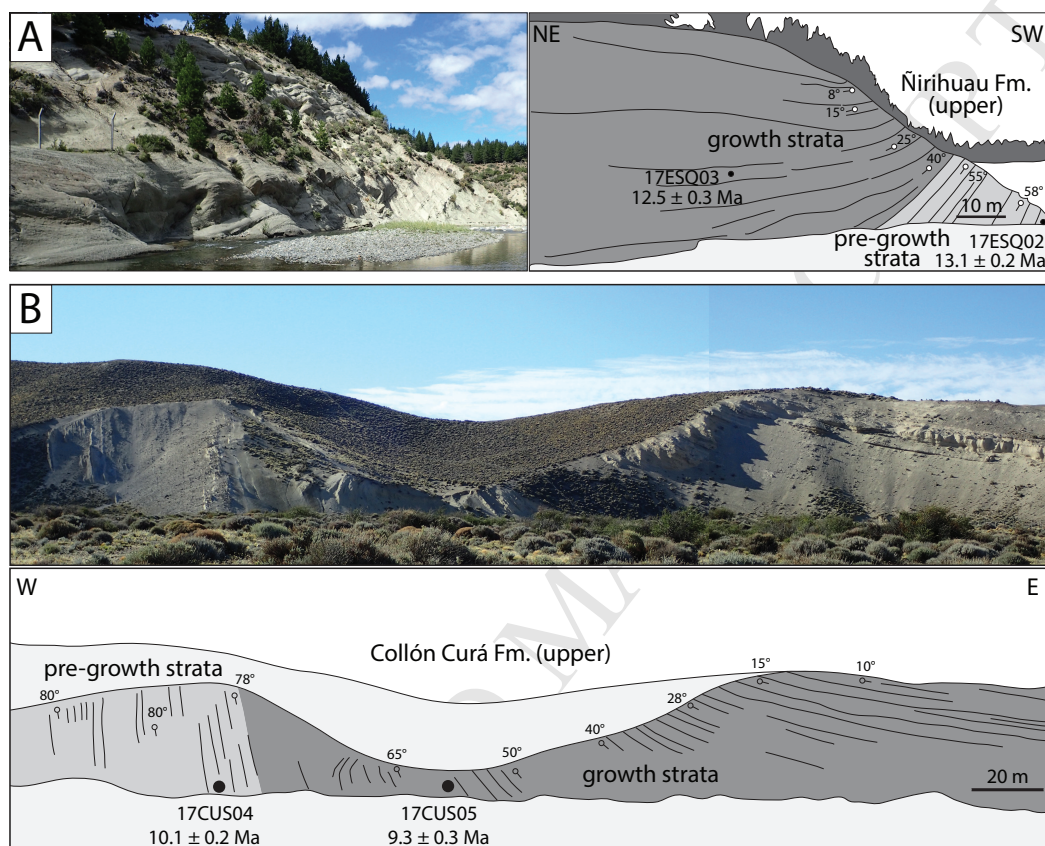
Butler et al., Figure 8
2 column width

Figure 8. Field photographs and line drawings of growth stratal packages in (A) the middle Miocene upper levels of the Ñirihuau Formation exposed in the Esquel Range of the North Patagonian foothills (after Echaurren et al., 2016) and (B) the late Miocene upper levels of the Collón Curá Formation in the broken foreland region adjacent to the Cordón del Maitén (after Ramos et al., 2015). Stratal dip values and maximum depositional ages (MDAs) for sandstone samples with young zircon U-Pb age populations (Fig. 5) are shown for pre-growth strata (light shading) and growth strata (dark shading).

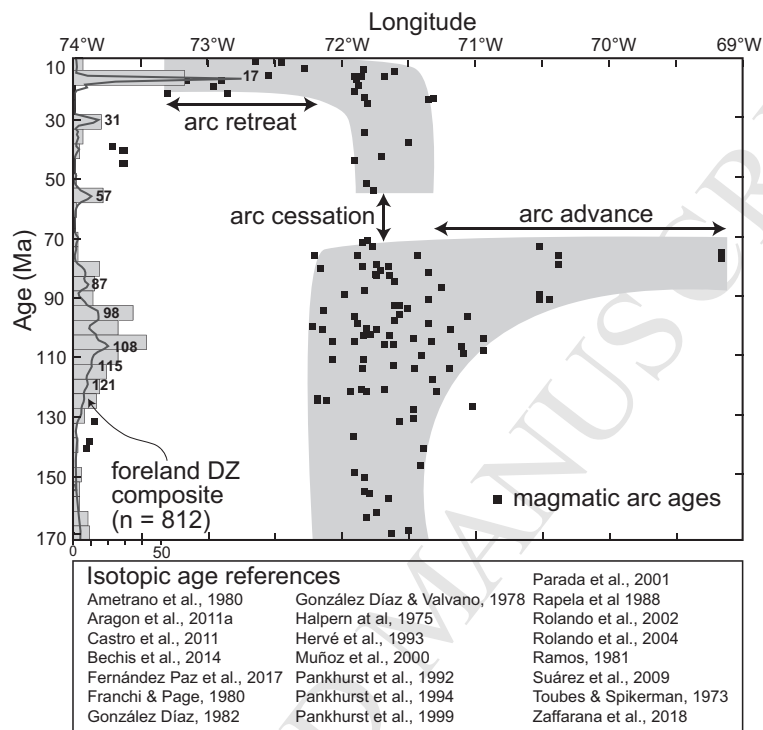
Butler et al., Figure 9
1.5 column width

Figure 9. Time-space plot showing the distribution of Middle Jurassic to Neogene (170–0 Ma) isotopic ages representing Andean arc magmatism at ~40–46°S. Detrital zircon U-Pb composite age data (below) for 200–0 Ma record in the Patagonian broken foreland. Arrows denote interpreted phases of arc advance (Campanian-Maastrichtian), arc cessation (Paleocene-Eocene), and arc retreat (middle-late Miocene).

Highlights: 3–5 points, <85 characters each

- (1) Detrital zircon U-Pb ages demonstrate Late Cretaceous reversal in sediment polarity
- (2) Depositional ages for growth strata constrain thrust-belt and intraforeland uplift
- (3) Hf isotopes record tectonic reorganization and overriding plate deformational mode